J|A|C|S
ARTICLES
Published on Web 07/24/2003

Cross-Modulation of the pK_a of Nucleobases in a Single-Stranded Hexameric-RNA Due to Tandem Electrostatic Nearest-Neighbor Interactions

P. Acharya, S. Acharya, P. Cheruku, N. V. Amirkhanov, A. Földesi, and J. Chattopadhyaya*

Contribution from the Department of Bioorganic Chemistry, Box 581, Biomedical Center, Uppsala University, SE-751 23 Uppsala, Sweden

Received February 13, 2003; E-mail: jyoti@boc.uu.se.

Abstract: The pH titration studies (pH 6.7−12.1) in a series of dimeric, trimeric, tetrameric, pentameric, and hexameric oligo-RNA molecules [GpA (**2a**), GpC (**3a**), GpApC (**5**), GpA^{1}pA^{2}pC (**6**), GpA^{1}pA^{2}pA^{3}pC (**7**), GpA^{1}pA^{2}pA^{3}pA^{4}pC (**8**)] have shown that the pK_a of N^1−H of 9-guaninyl could be measured not only from its own δH8G, but also from the aromatic marker protons of other constituent nucleobases. The relative chemical shift differences [$\Delta\delta_{(N-D)}$] between the protons in various nucleotide residues in the oligo-RNAs at the neutral (N) and deprotonated (D) states of the guanine moiety show that the generation of the 5′-(9-guanylate ion) in oligo-RNAs **2**−**8** reduces the stability of the stacked helical RNA conformation owing to the destabilizing anion(G$^-$)−π/dipole(Im$^{\delta-}$) interaction. This destabilizing effect in the deprotonated RNA is, however, opposed by the electrostatically attractive atom−$\pi\sigma$ (major) as well as the anion(G$^-$)−π/dipole-(Py$^{\delta+}$) (minor) interactions. Our studies have demonstrated that the electrostatically repulsive anion(G$^-$)−π/dipole(Im$^{\delta-}$) interaction propagates from the first to the third nucleobase quite strongly in the oligo-RNAs **6**−**8**, causing destacking of the helix, and then its effect is gradually reduced, although it is clearly NMR detectable along the RNA chain. Thus, such specific generation of a charge at a single nucleobase moiety allows us to explore the relative strength of stacking within a single-stranded helix. The pK_a of 5′-**G**p residue from its own δH8G in the hexameric RNA **8** is found to be 9.76 ± 0.01; it, however, varies from 9.65 ± 0.01 to 10.5 ± 0.07 along the RNA chain as measured from the other marker protons (H2, H8, H5, and H6) of 9-adeninyl and 1-cytosinyl residues. This nucleobase-dependent modulation of pK_as (ΔpK_a ± 0.9) of 9-guaninyl obtained from other nucleobases in the hexameric RNA **8** represents a ΔG°_{pKa} difference of ca. 5.1 kJ mol^{-1}, which has been attributed to the variable strength of electrostatic interactions between the electron densities of the involved atoms in the offset stacked nucleobases as well as with that of the phosphates. The chemical implication of this variable pK_a for guanin-9-yl deprotonation as obtained from all other marker protons of each nucleotide residue within a ssRNA molecule is that it enables us to experimentally understand the variation of the electronic microenvironment around each constituent nucleobase along the RNA chain in a stepwise manner with very high accuracy without having to make any assumption. This means that the pseudoaromaticity of neighboring 9-adeninyl and next-neighbor nucleobases within a polyanionic sugar−phosphate backbone of a ssRNA can vary from one case to another due to cross-modulation of an electronically coupled π system by a neighboring nucleobase. This modulation may depend on the sequence context, spatial proximity of the negatively charged phosphates, as well as whether the offset stacking is ON or OFF. The net outcome of this electrostatic interaction between the neighbors is creation of new sequence-dependent hybrid nucleobases in an oligo- or polynucleotide whose properties are unlike the monomeric counterpart, which may have considerable biological implications.

Introduction

The self-assembly process of DNA and RNA is mainly dictated by stacking and hydrogen-bonding interactions. Stacking interactions between two neighboring nucleobases stabilize the DNA or RNA helix[1a,2] by ca. 0.4−3.6 kcal mol^{-1}, whereas H-bonding promoted stabilization can vary from 0.5 to 2 kcal mol^{-1} per H bond.[1] It is, however, the stacking interaction that plays a more important role in the self-assembly of the single-stranded RNA structures, which is important for both the

(1) (a) Saenger, W. *Principles of Nucleic Acid Structure*; Springer-Verlag, Berlin, 1988. (b) Bloomfield, V. A.; Crothers, D. M.; Tinoco, I. *Nucleic Acids: Structures, Properties and Functions*, University Science Books, Sausalito, CA, 1999.

(2) (a) Burkard, M. E.; Kierzek, R.; Turner, D. H. *J. Mol. Biol.* **1999**, *290*, 967 and references therein. (b) Kim, J.; Walter, A. E.; Turner, D. H. *Biochemistry* **1996**, *35*, 13753. (c) Bommarito, S.; Peyret, N.; SantaLucia, J., Jr. *Nucleic Acids Res.* **2000**, *28*, 1929. (d) Rosemeyer, H.; Seela, F. *J. Chem. Soc., Perkin Trans. 2* **2002**, 746. (e) Ohmichi, T.; Nakano, S.-i.; Miyoshi, D.; Sugimoto, N. *J. Am. Chem. Soc.* **2002**, *124*, 10367. (f) Zhu, J.; Wartell, R. M. *Biochemistry* **1997**, *36*, 15326. (g) Zhu, J.; Wartell, R. M. *Biochemistry* **1999**, *38*, 15986. (h) The importance of stacking has been identified in DNA polymerase activity and in efficiency of DNA synthesis. For review: Kool, E. T. *Annu. Rev. Biophys. Biomol. Struct.* **2001**, *30*, 1 and references therein.

10.1021/ja034651h CCC: $25.00

recognition and interaction with many ligands including proteins. A single dangling nucleotide[2a−d] at the end of both DNA and RNA duplexes is known to increase the duplex stability. In more recent studies,[2e] it has been shown that longer single-stranded dangling residues (up to tetranucleotide) stabilize the RNA−RNA and DNA−DNA duplexes even slightly more (by an extra ∼0.1−1.0 kcal mol^{-1}) than the single-nucleotide dangling end, which is reported to be ∼2.0 kcal mol^{-1}. This enhanced stability arising from the long dangling ends originates from the single-stranded stacking interaction. The biological importance of the dangling nucleotides in RNA function is quite ubiquitous: the dangling 5′-ACCA-3′ at the 3′-terminus of tRNA orchestrates the aminoacylation reaction for protein synthesis in the ribosome. The high fidelity of this protein synthesis in the ribosome is dictated by the specific codon−anticodon interaction between mRNA and tRNA, which is stabilized by the dangling ends. It has also been shown[2e] that 2−3nt dangling ends are important for the RNAi functionality. A dangling nucleotide at the 3′-end of a pseudoknot RNA is also known to stabilize the stem structure. Recently, it has been demonstrated that single unpaired base bulges in RNA duplexes enhance the stability of the RNA more compared to the fully base-paired counterpart, in which both the base identity as well as the nearest-neighbor context have been shown to be important for the overall relative stability of the bulges.

Although much is known in qualitative terms about the ubiquitous role of stacking in dictating the geometry and function of nucleic acids in general,[13] very little direct experimental evidence is available on the molecular nature of stacking interactions.

More direct experimental evidences are, however, available from the studies of aromatic interactions in the nonbiological systems,[5−7] which are of considerable fundamental interest in understanding molecular recognition and in the modeling of the biological functionalities. The major noncovalent aromatic interactions (mostly in nonbiological model systems) so far identified can be categorized as (i) $\pi-\pi$ interaction [face-to-face, edge-to-face (T-shaped), and offset (atom$-\pi\sigma$)],[5,6] (ii) CH$-\pi$ interaction (involving CH of both aryl[6c,e−g] and alkyl[7i,8c]), and (iii) ion$-\pi$ interaction (involving both cation$-\pi$[7h] as well as anion$-\pi$[10]).

Evidences regarding the nature of intramolecular aromatic interactions in nucleic acids and their complexes[3,8] have mainly come from various structural studies: Thus, Hunter et al. first invoked the presence of offset stacked nucleobases in DNA[5a,b] based on the X-ray crystallographic data followed by computer modeling to construct conformation-dependent energy maps based on van der Waals and electrostatic interactions calculated between stacked bases. Rooman et al.[8b] defined and analyzed stair-shaped motifs, which simultaneously involve base stacking, hydrogen bond, and cation$-\pi$ interaction in protein−DNA complexes through the geometrical proximity found in the X-ray crystallographic database. Recent database studies[8c] showed the importance of thymine−methyl/π interaction in the sequence-dependent deformability of DNA. Moreover, studies based on screening of nucleic acid databases showed that divalent cations [like $Mg(OH_2)_6^{2+}$] interact favorably with π systems of nucleic acid bases.[8a] Thus, the hydrated magnesium ions located in the major groove of B-DNA pull cytosine bases partially out from the helical stack, exposing π systems to positive charge. It is also found that some critical cation$-\pi$ interactions contribute to the stability of the anticodon arm of yeast tRNA^{phe} and to the magnesium core of the Tetrahymena group I intron P4−P6

(3) (a) Hsu, P.; Hodel, M. R.; Thomas, W. J.; Talyor, L. J.; Hagedorn, C. H.; Hodel, A. E. *Biochemistry* **2000**, *39*, 13730. (b) Hu, G.; Gershon, P. D.; Hodel, A. E.; Quiocho, F. A. *Proc. Natl. Acad. Sci. U.S.A.* **1999**, *96*, 7149. (c) Hu, G.; Oguro, A.; Li, C.; Gershon, P. D.; Quiocho, F. A. *Biochemistry* **2002**, *41*, 7677.

(4) (a) Ossipov, D.; Zamaratski, E.; Chattopadhyaya, J. *Nucleosides Nucleotides* **1998**, *17*, 1613. (b) Maltseva, T. V.; Agback, P.; Repkova, M. N.; Venyaminova, A. G.; Ivanova, E. M.; Sandström, A.; Zarytova, V. F.; Chattopadhyaya, J. *Nucleic Acids Res.* **1994**, *22*, 5590. (c) Ossipov, D.; Pradeepkumar, P. I.; Holmer, M.; Chattopadhyaya, J. *J. Am. Chem. Soc.* **2001**, *123*, 3551. (d) Acharya, S.; Acharya, P.; Földesi, A.; Chattopadhyaya, J. *J. Am. Chem. Soc.* **2002**, *124*, 13722. (e) Acharya, P.; Acharya, S.; Földesi, A.; Chattopadhyaya, J. *J. Am. Chem. Soc.* **2003** *125*, 2094. (f) In our earlier study (ref 4e) with the dimer (GpA, **2a**) and the trimers, GpApA (**4**) and GpApC (**5**), we found that none of the H2A showed any appreciable chemical shift change as a function of pH ($\Delta\delta_{N-D}$), except for H2A of p**A**p of **4**, which became clearly shielded**,** whereas all H8 were deshielded because of destacking (see Figure 3 of this paper). This H2A shielding was explained on the basis of a T-shaped interaction between the pyrimidine of pAp and the 9-gunainyl ion in ref 4e. The review of the data in context with the larger oligo-RNAs (Figure 3 of this paper), however, suggests that we cannot rule out an attractive atom$-\pi\sigma$ and anion(G^-)$-\pi$/dipole-($Py^{\delta+}$) interaction for the pyrimidine of p**A**^{1}p of **4** and the 9-gunainyl ion interaction causing shielding of H2A of of p**A**p of **4**, whereas the deshielding of H8A can be explained by a destacking owing to anion(G^-)$-\pi$/dipole-($Im^{\delta-}$) repulsion. (g) The electrostatic/charge-transfer interaction (or donor−accpetor properties) has been invoked to explain the observed results in the pH-dependent studies of dimeric RNA.[4d] However, the present study on oligo-RNAs of various chain lengths points to the fact that electrostatics is the dominant component in these base−base interactions in both neutral and ionic states. Observation of modulation of pK_a of 9-guaninyl from the marker protons of the neighboring bases (refs 4d,e and this paper), however, suggests a possible contribution of charge transmission between them (but no charge-transfer band in UV is, however, found). Thus, it is not possible at this stage to delineate the relative contribution of electrostatic and nonelectrostatic components in our observed overall interactions in RNA. There are two primary reasons for this: (i) our RNA system is too large for a high basis-set ab initio optimization, no well-defined starting geometry of ssRNA is available for this purpose, and (ii) we cannot use any other solvent but water for solubility reasons for examining the relative contribution of electrostatics as delineated in earlier studies.[6h,i] The study of the effect of salt concentration, however, may allow us (although it is known to be minimal for single-strand nucleic acid stacking[1b]) to dissect the origin of electrostatics vs unusual pK_a values from various factors such as hydrogen bond, charge−charge interaction, and the degree of solvent exposure of the charged group.[4h−j] (h) Song, J.; Laskowski, M., Jr.; Qasim, M. A.; Markley, J. L. *Biochemistry* **2003**, *42*, 2847. (i) Livesay, D. R.; Zambeck, P.; Rojnuckarin, A.; Subramaniam, S. *Biochemistry* **2003**, *42*, 3464. (j) Consonni, R.; Arosio, I.; Belloni, B.; Fogolari, F.; Fusi, P.; Shehi, E.; Zetta, L. *Biochemistry* **2003** *42, 1421*.

(5) (a) Hunter, C. A. *J. Mol. Biol*. **1993**, *230*, 1025 and references therein. (b) Packer, M. J.; Dauncey, M. P.; Hunter, C. A. *J. Mol. Biol*. **2000**, *295*, 71. (c) For review: Hunter, C. A.; Lawson, K. R.; Perkins, J.; Urch, C. J. *J. Chem. Soc., Perkin Trans. 2* **2001**, 651. (d) Hunter, C. A.; Sanders, J. K. M. *J. Am. Chem. Soc*. **1990**, *112*, 5525. (e) Packer, M. J.; Hunter, C. A. *J. Am. Chem. Soc*. **2001**, *123*, 7399.

(6) (a) The experimental evidence showed that the magnitude of offset stacking interactions is dictated by the geometry of the stacked components, which, in turn, is influenced by the nature of ring substituents. Rashkin, M. J.; Waters, M. L. *J. Am. Chem. Soc*. **2002**, *124*, 1860 and refs 1, 2, and 8 therein. (b) Newcomb, L. F.; Gellman, S. H. *J. Am. Chem. Soc*. **1994**, *116*, 4993. (c) Kim, E.; Paliwal, S.; Wilcox, C. S. *J. Am. Chem. Soc*. **1998**, *120*, 11192. (d) Jennings, W. B.; Farrell, B. M.; Malone, J. F. *Acc. Chem. Res.* **2001**, *34*, 885. (e) Cozzi, F.; Cinquini, M.; Annuziata, R.; Siegel, J. S. *J. Am. Chem. Soc*. **1993**, *115*, 5330. (f) Cozzi, F.; Cinquini, M.; Annuziata, Dwyer, T.; R.; Siegel, J. S. *J. Am. Chem. Soc*. **1992**, *114*, 5729. (g) Cozzi, F.; Annuziata, R.; Benaglia, M.; Cinquini, M.; Rainmondi, L.; Baldridge, K. K.; Siegel, J. S. *Org. Biomol. Chem.* **2003**, *1*, 157. (h) Waters, M. *Curr. Opin. Chem. Biol*. **2002**, *6*, 736 and references therein. (i) Shetty, A. S.; Zhang, J. S.; Moore, J. S. *J. Am. Chem. Soc*. **1996**, *118*, 1019.

(7) (a) Ishida, T.; Shibata, M.; Fuji, K.; Inoue, M. *Biochemistry* **1983**, *22*, 3571. (b) Ribas, J.; Cubero, E.; Luque, J.; Orozco, M. *J. Org. Chem*. **2002**, *67*, 7057. (c) Schmidt, A.; Kindermann, M. K.; Vainotalo, P.; Nieger, M. *J. Org. Chem*. **1999**, *64*, 9499. (d) Allwood, B. L.; Shahriari-Zavareh, H.; Stoddart, J. F.; Williams, D. J. *J. Chem. Soc., Chem. Commun*. **1987**, 1058. (e) Philip, D.; Slawin, A. M. Z.; Spencer, N.; Stoddart, J. F.; Williams, D. J. *J. Chem. Soc., Chem. Commun.* **1991**, 1584. (f) Nicolas, L.; Beugelmans-Verrier, M.; Guilhem, J. *Tetrahedron* **1981**, *37*, 3847. (g) Doughterty, D. A.; Stauffer, D. A. *Science* **1990**, *250*, 1558. (h) For review on cation$-\pi$ interaction, see: Ma, J. C.; Doughterty, D. A. *Chem. Rev*. **1997**, *97*, 1303. (i) For substituent effect on alkyl (CH)$-\pi$ interaction, see: Suezawa, H.; Hashimoto, T.; Tsuchinaga, K.; Yoshida, T.; Yuzuri, T.; Sakakibara, K.; Hirota, M.; Nishio, M. J. *J. Chem. Soc., Perkin Trans. 2* **2000**, 1243. (j) Ferguson, S. B.; Seward, E. M.; Diederich, F.; Sanford, E. M.; Chou, A.; Inocencio-Szweda, P.; Knobler, C. B. *J. Org. Chem*. **1988**, *53*, 5593.

domain. Such cation−π interactions have been also implicated in DNA bending, DNA−protein recognition, base-flipping, RNA folding, and catalysis.[8a] Ab initio studies have shown the presence of the aromatic interactions (mostly of cation−π in nature)[8i] between protein and DNA involving positively charged Arg or Lys side chains and aromatic rings of nucleic acids. The X-ray studies along with calorimetric and fluorescence analyses have shown[3] the importance of electrostatic cation−π interaction in the protein recognition of the m^7G part of the mRNA cap structure. Similar kinetic and calorimetric experiments[8e] have also identified the key aromatic $\pi-\pi$ stacking interaction between Tyr41 and the adenine ring of bound nucleotides in the active site of an aminoglycoside phosphotransferase enzyme.

Our studies,[4d,e] on the other hand, deal with the experimental demonstration of the ubiquitous electrostatic interactions among the nearest-neighbor pseudoaromatic nucleobases in oligo-RNA in both the neutral as well the ionic states, modeling ligand binding to nucleic acid bases. The pH-dependent NMR studies[4d] of di-ribonucleoside (3′ → 5′) monophosphates compared to their corresponding monomers showed that each nucleobase in a dimer not only shows its own pK_a but also that of the neighboring nucleobase, owing to the cross-modulation of each other's pseudoaromatic character in an electronically coupled π system via intramolecular electrostatic interaction through offset stacking. Thus, the physicochemical comparison, for example, of the GpA/G^-pA and ApG/ApG^- showed the nature of atom−$\pi\sigma$[5,9] versus anion−π[10] interactions, whereas the comparison in the two isomeric dimers[4d,f] in the neutral, anionic, and cationic states [UpA/U^-pA/UpA^{H+} and ApU/ApU^-/A^{H+}-pU, or UpC/U^-pC/UpC^{H+} and CpU/CpU^-/C^{H+}pU] showed direct evidence[4g] of the electrostatic interaction between the neighboring nucleobases (atom−$\pi\sigma$[5] in the neutral state, anion−π[10] in the deprotonated state vs cation−π[7g,h] in the protonated state) as a result of intramolecular offset stacking. This electrostatic interaction leads to almost total modulation of the pseudoaromaticity by nearly total transmission of ΔG°_{pKa}[14a−c,f−i] from one nucleobase to the nearest neighbor (16−53 kJ mol^{-1}, depending upon whether the nucleobase is at the cationic or anionic state). This suggested that the nucleobase in a stacked dinucleotide, unlike simple monomers, constitutes an electronically coupled heterocyclic system. Similarly, we demonstrated[4e] the existence of this electrostatic nearest-neighbor interaction between the first and third nucleobases in tri-ribonucleoside(3′ → 5′)diphosphates with ΔG°_{pKa} transmission from the 5′-guanylate ion to the 3′-end nucleobase via the central adenin-9-yl, 55−56 kJ mol^{-1} in each step through a distance spanning ∼6.8 Å in an unfolded state. As a result, we found[4e] that the pK_a of guanin-9-yl moiety has become 9.25 ± 0.02 in **G**pEt (**1a**), 9.17 ± 0.02 in **G**pA (**2a**), 9.75 ± 0.02 in **G**pApA (**3**), and 9.88 ± 0.03 in **G**pApC (**4**), which meant that the 9-guaninyl moiety of trimers is more basic than that in the monomer or in the dimer because of both the neighboring nucleobases and the phosphate(s).

Here we show that the stabilizing electrostatic atom−$\pi\sigma$ interaction,[5] indeed, extends from the first to the sixth nucleotide in a single-stranded hexameric RNA, which is ∼21 Å apart in the unfolded neutral state. We also present evidence showing that, in the deprotonated state, the stability of the stacked helical

(8) Studies showing the importance of the weak noncovalent aromatic interactions in biological functionalities: (a) McFail-Isom, L.; Shui, X.; Williams, L. D. *Biochemistry* **1998**, *37*, 17105. (b) Rooman, M.; Liévin, J.; Buisine, E.; Wintjens R. *J. Mol. Biol.* **2002**, *319*, 67. (c) Umezawa, Y.; Nishio, M. *Nucleic Acids Res.* **2002**, *30*, 2183. (d) Zacharias, N.; Dougherty, D. *Trends Pharm. Sci.* **2002**, *23*, 281 and references therein. (e) Boehr, D. D.; Farley, A. R.; Wright, G. D.; Cox, J. R. *Chem. Biol.* **2002**, *9*, 1209. (f) Tatko, C. D.; Waters, M. L. *J. Am. Chem. Soc.* **2002**, *124*, 9372. (g) Butterfield, S. M.; Patel, P. R.; Water, M. L. *J. Am. Chem. Soc.* **2002**, *124*, 9751. (h) Tsou, L. K.; Tatko, C. D.; Waters, M. L. *J. Am. Chem. Soc.* **2002**, *124*, 14917. (i) Gervasio, F. L.; Chelli, R.; Procacci, P.; Schettino, V. *Proteins: Struct., Funct., Genet.* **2002**, *48*, 117. (j) Zhou, Z.; Swenson, R. P. *Biochemistry* **1996**, *35*, 15980. (k) Gallivan, J. P.; Dougherty, D. *Proc. Natl. Acad. Sci. U.S.A.* **1999**, *96*, 9459. (l) Biot, C.; Buisine, E.; Kwasigroch, J.-M.; Wintjens, R.; Rooman, M. *J. Biol. Chem.* **2002**, *277*, 40816.

(9) The intra- and intermolecular stacking and/or other aromatic interactions[5−8] involving both biological as well as nonbiological systems has been shown to be a major force in molecular recognition and biological functionalities. The aromatic stacking interaction between nucleobases[2h] in water has been implicated to electrostatic effects (dipole−dipole and dipole−induced dipole) interactions, dispersion (momentary dipole−induced dipole), and solvation. Hunter et al.[5] invoked offset stacking involving attractive atom−$\pi\sigma$ interaction (electrostatic in nature) and edge-to-face interactions (same as center-to-edge termed by Siegel et al.[6g]) rather than energetically unfavorable $\pi-\pi$ interaction as in face-to-face stacking between two aromatic moieties. In both offset stacking and edge-to-face interactions, the CH group of the edge ring and the electron density of the face ring are sensitive to changes in the local charge (partial charge) distribution of the two rings.[5c,6g] However, unlike offset stacking, edge-to-face interaction is considered as weak noncovalent through-space aromatic interaction, not any stacking interaction.[6a] Theoretical studies[7b] recently showed that dispersion effects other than electrostatics dominate both aryl CH−π, and alkyl CH−π interactions. In all cases alkyl CH−π interactions are weaker than aryl CH−π interactions. Nishio et al.[7i] proposed partial charge transfer arising from through-space proximity between alkyl hydrogen and aromatic moiety as the basis for CH−π interaction. On the other hand, Siegel et al.[6e−g] and Diedrich et al.[7j] proposed a through-space polar (Coulombic)/π contribution as a dominating factor in the electrostatic interactions involved in edge-to-face as well as the center-to-edge (i.e., offset) oriented aromatic moieties in the neutral[7e] as well as in the ionic states (such as carboxylate ion/arene[7f] and trimethylammonium ion/arene[7f] interaction). Moreover, Dougherty et al. showed[7g,h] that both electrostatic and polarization effects are dominant contributions in the cation−π interaction, which have been shown[8f−h] to make a significant contribution in the stabilization of α-helical peptides in aqueous solution. Recent works have also shown theoretical evidences[10] of anion−π interactions.

(10) (a) Recent studies[10a−d] invoked a weak noncovalent attractive anion−π interaction involving the negatively charged π cloud of unsubstitued benzene ring and positively charged σ framework of the hexafluorobenzene (C_6F_6). However, recent studies[10f] proposed an anion−arene interaction having both a positive as well as a negative component. (b) Garau, C.; Quinonero, D.; Frontera, A.; Ballester, P.; Costa, A.; Deya, P. M. *New J. Chem.* **2003**, *27*, 211. (c) Quinonero, D.; Garau, C.; Rotger, C.; Frontera, A.; Ballester, P.; Costa, A.; Deya, P. M. *Angew. Chem., Int. Ed.* **2002**, *41*, 3389. (d) Quinonero, D.; Garau, C.; Frontera, A.; Ballester, P.; Costa, A.; Deya, P. M. *Chem. Phys. Lett.* **2002**, *359*, 486. (e) Mascal, M.; Armstrong, A.; Bartberger, M. D. *J. Am. Chem. Soc.* **2002**, *124*, 6274. (f) Gale, P.; Navakhun, K.; Camiolo, S.; Light, M. E.; Hursthouse, M. *J. Am. Chem. Soc.* **2002**, *124*, 11228.

(11) (a) Thibaudeau, C.; Plavec, J.; Chattopadhyaya, J. *J. Org. Chem.* **1996**, *61*, 266. (b) Acharya, P.; Trifonova, A.; Thibaudeau, C.; Földesi, A.; Chattopadhyaya, J. *Angew. Chem., Int. Ed. Engl.* **1999**, *38*, 3645. (c) For review, see: Thibaudeau, C.; Chattopadhyaya, J. *Stereoelectronic Effects in Nucleosides and Nucleotides and their Structural Implications*; Department of Bioorganic Chemistry, Uppsala University Press (jyoti@boc.uu.se); Sweden, 1999 (ISBN 91-506-1351-0) and references therein.

(12) (a) Narlikar, G. J.; Herschlag, D. *Annu. Rev. Biochem.* **1997**, *66*, 19 and references therein. (b) Legault, P.; Pardi, A. *J. Am. Chem. Soc.* **1997**, *119*, 6621 and references therein. (c) Cech, T. R. *Annu. Rev. Biochem.* **1990**, *59*, 543. (d) DeRose, V. J. *Chem. Biol.* **2002**, *9*, 961. (e) Lilley, D. M. J. *ChemBioChem* **2001**, 2, 729. (f) Yoshida, A.; Shan, S.; Herschlag, D.; Piccirilli, J. *Chem. Biol.* **2000**, *7*, 85.

(13) (a) Chan, S. I.; Nelson, J. H. *J. Am. Chem. Soc.* **1969**, *91*, 168. (b) Altona, C. In *Structure and Conformation of Nucleic Acids and Protein- Nucleic Acid Interactios*; Sundaralingam, M., Rao, S. T., Eds.; University Park Press: Baltimore, MD, 1975; p 613. (c) Lee, C.-H.; Ezra, F. S.; Kondo, N. S.; Sarma, R. H.; Danyluk, S. *Biochemistry* **1976**, *15*, 3627. (d) Olsthoorn, C. S. M.; Bostelaar, L. J.; de Rooij, J. F. M.; van Boom, J. H. *Eur. J. Biochem.* **1981**, *115*, 309. (e) Simpkins, H.; Richards, E. G. *Biochemistry* **1967**, *6*, 2513.

(14) (a) The equation $\Delta G^\circ_{pKa} = 2.303RTpK_a$ has been used[14b,c,f−i] to estimate the free energy of protonation for compounds **1**−**8**. (b) Perrin, D. D.; Dempsey, B.; Serjeant, E. P. *pK$_a$ prediction for organic acids and bases*; Chapman and Hall: New York, 1981. (c) Sharp, K. A.; Honig, B. *Annu. Rev. Biophys. Chem.* **1990**, *19*, 301. (d) Tso, P. O. P. *Basic Principles in Nucleic Acid Chemistry*; Academic Press: New York and London, 1974; Vol. 1, p 469. (e) Wyman, J.; Gill, S. J. *Binding and Linkage−Functional Chemistry of Biological Macromolecules*; University Science Books: Mill Valley, CA, 1990. (f) Urry, D. W.; Gowda, D. C.; Peng, S. Q.; Parker, T. M. *Chem. Phys. Lett.* **1995**, *239*, 67. (g) Shi, Z.; Krantz, B. A.; Kallenbach, N.; Sosnick, T. R. *Biochemistry* **2002**, *41*, 2120. (h) Tollinger, M.; Crowhurst, K. A.; Kay, L. E.; Forman-Kay, J. D. *PNAS* **2003**, *100*, 4545. (i) Sancho, J.; Serrano, L.; Fersht, A. R. *Biochemistry* **1992**, *31*, 2253.

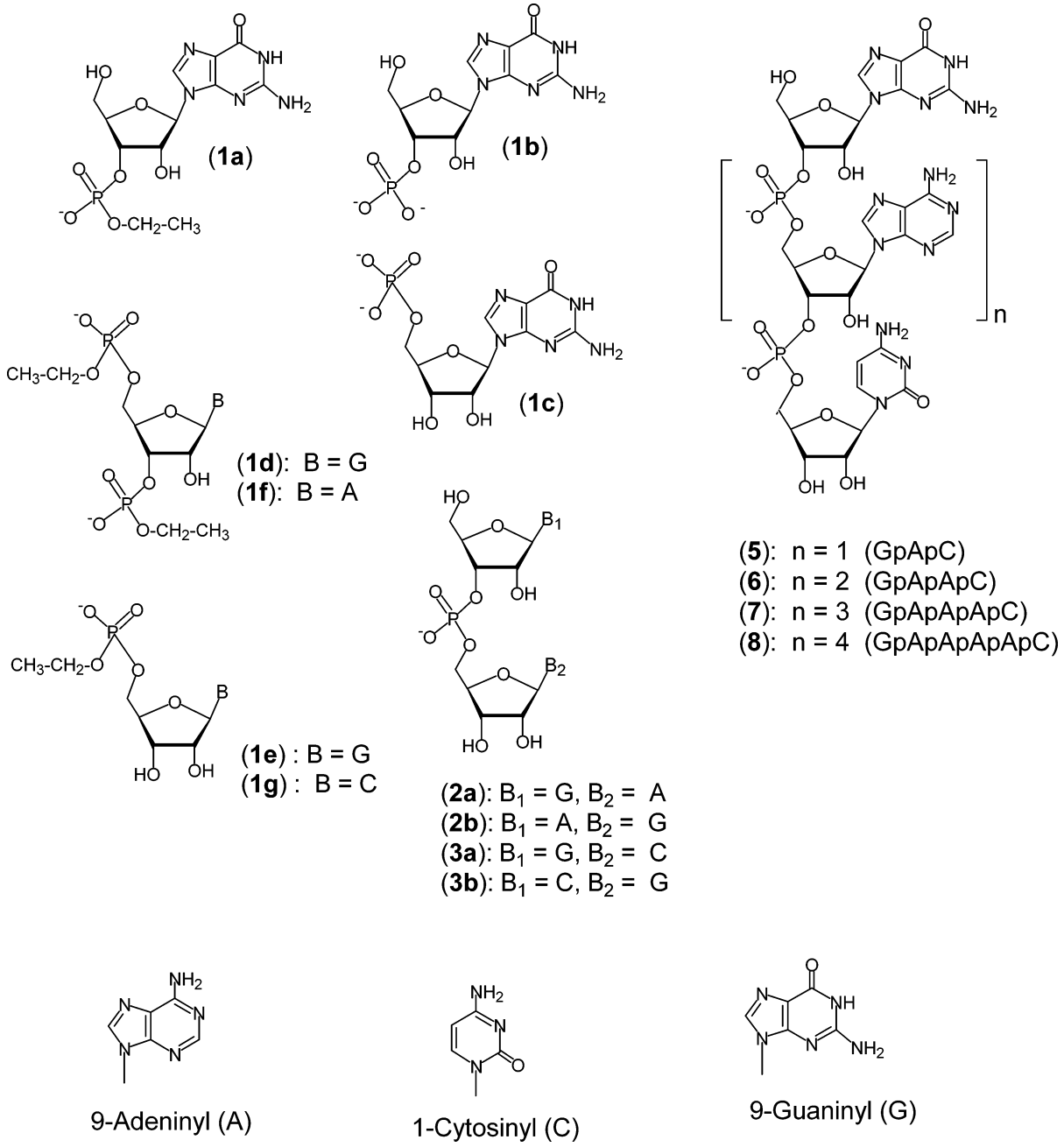

Figure 1. Compounds used in this study: GpA (**2a**), ApG (**2b**), GpC (**3a**), CpG (**3b**), GpApA (**4**)[4e] (not shown), GpApC (**5**), GpA^{1}pA^{2}pC (**6**), GpA^{1}pA^{2}pA^{3}pC (**7**), and GpA^{1}pA^{2}pA^{3}pA^{4}pC (**8**) and their monomeric counterparts GpEt (**1a**), 3′-GMP (**1b**), 5′-GMP (**1c**), EtpGpEt (**1d**), 5′-EtpG (**1e**), EtpApEt (**1f**), and 5′-EtpC (**1g**). Note monomeric compounds **1a**−**f** are used as reference compounds to evaluate the relative stacking in oligo-RNAs **2a**−**8**.

RNA conformation is reduced by the destabilizing anion(G^-)−π/dipole($Im^{\delta-}$) interaction owing to the generation of the 5′-(9-guanylate ion) (for terminologies used in various electrostatic interactions, see ref 9). This destabilizing effect in the deprotonated RNA is, however, opposed by the attractive atom−$\pi\sigma$ interaction (major) as well as the minor anion(G^-)−π/dipole-($Py^{\delta+}$) interactions.

Results and Discussion

(A) Effect of Generation of the 5′-Guanylate Ion and Its Electrostatic Modulation in the Hexameric ssRNA. The pH titration studies (pH 6.7−12.1) in a series of dimeric, trimeric, tetrameric, pentameric, and hexameric single stranded (ss) oligo-RNA molecules [GpA (**2a**), GpC (**3a**), GpA^{1}pA (**4**)[4e], GpApC (**5**), GpA^{1}pA^{2}pC (**6**), GpA^{1}pA^{2}pA^{3}pC (**7**), GpA^{1}pA^{2}pA^{3}pA^{4}pC (**8**)] (Figure 1) are designed such that only a single anionic species at the N^1 of the 9-guaninyl moiety can be generated in the alkaline pH in these RNA molecules **2**−**8**. It is aimed to show how far the electrostatic modulation of the 9-guanylate ion in this electronically coupled system, as an interplay of Coulombic attractive or repulsive forces, propagates through the intervening p**A**p nucleotide moieties until the terminal p**C**-3′ residue in comparison with the neutral counterpart. We reasoned that the footprint of this propagation of the electrostatic forces among the neighboring nucleobases will be evident by a change of the chemical environment (i.e., chemical shifts) around their aromatic marker protons (δH2A, δH8A, δH5C, and δH6C) owing to a change of the stacking orientation and/

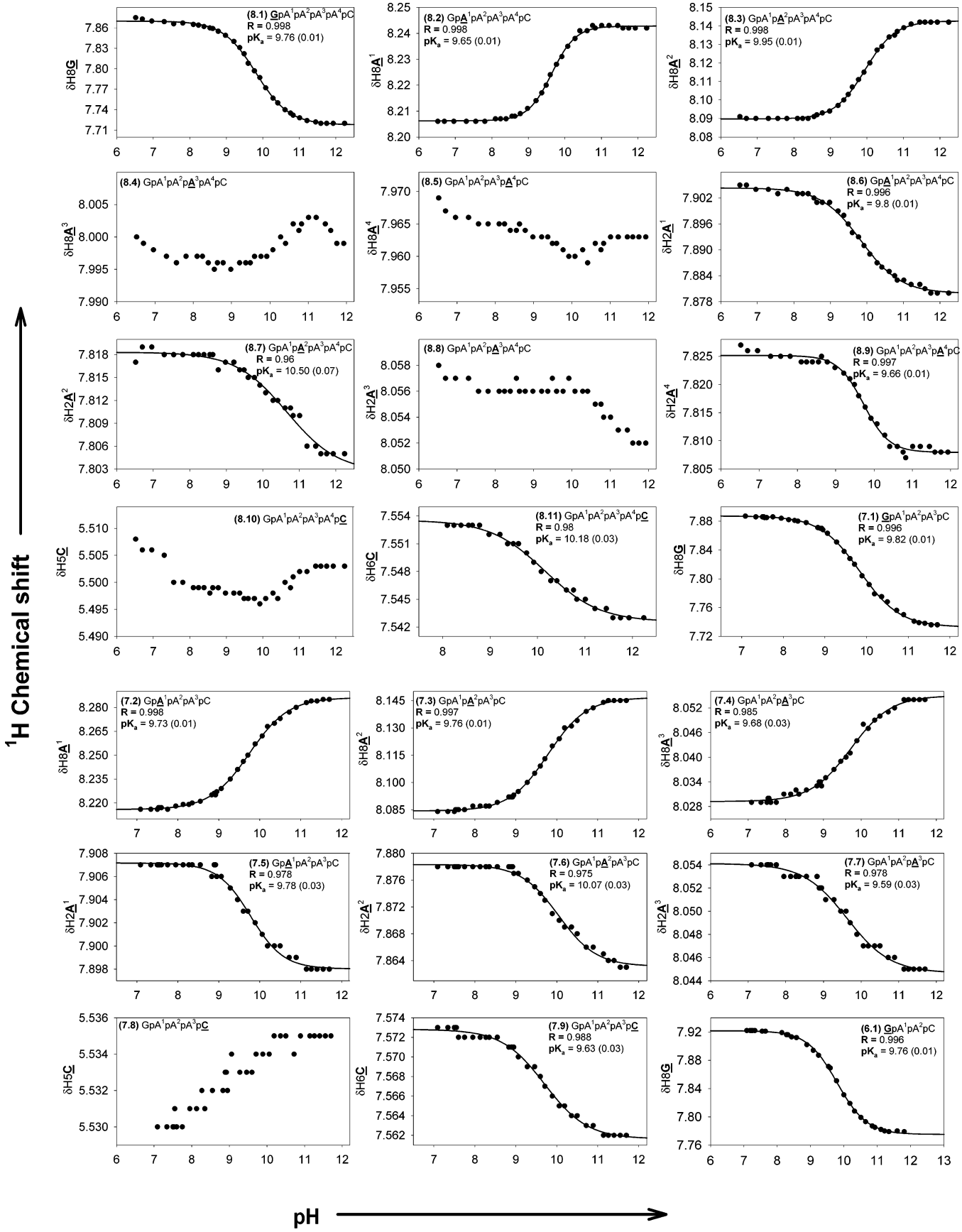
(8.1) GpA1pA2pA3pA4pC
R = 0.998
pKa = 9.76 (0.01)
δH8G
(8.2) GpA1pA2pA3pA4pC
R = 0.998
pKa = 9.65 (0.01)
δH8A1
(8.3) GpA1pA2pA3pA4pC
R = 0.998
pKa = 9.95 (0.01)
δH8A2
(8.4) GpA1pA2pA3pA4pC
δH8A3
(8.5) GpA1pA2pA3pA4pC
δH8A4
(8.6) GpA1pA2pA3pA4pC
R = 0.996
pKa = 9.8 (0.01)
δH2A1
(8.7) GpA1pA2pA3pA4pC
R = 0.96
pKa = 10.50 (0.07)
δH2A2
(8.8) GpA1pA2pA3pA4pC
δH2A3
(8.9) GpA1pA2pA3pA4pC
R = 0.997
pKa = 9.66 (0.01)
δH2A4
(8.10) GpA1pA2pA3pA4pC
δH5C
(8.11) GpA1pA2pA3pA4pC
R = 0.98
pKa = 10.18 (0.03)
δH6C
(7.1) GpA1pA2pA3pC
R = 0.996
pKa = 9.82 (0.01)
δH8G
(7.2) GpA1pA2pA3pC
R = 0.998
pKa = 9.73 (0.01)
δH8A1
(7.3) GpA1pA2pA3pC
R = 0.997
pKa = 9.76 (0.01)
δH8A2
(7.4) GpA1pA2pA3pC
R = 0.985
pKa = 9.68 (0.03)
δH8A3
(7.5) GpA1pA2pA3pC
R = 0.978
pKa = 9.78 (0.03)
δH2A1
(7.6) GpA1pA2pA3pC
R = 0.975
pKa = 10.07 (0.03)
δH2A2
(7.7) GpA1pA2pA3pC
R = 0.978
pKa = 9.59 (0.03)
δH2A3
(7.8) GpA1pA2pA3pC
δH5C
(7.9) GpA1pA2pA3pC
R = 0.988
pKa = 9.63 (0.03)
δH6C
(6.1) GpA1pA2pC
R = 0.996
pKa = 9.76 (0.01)
δH8G
1H Chemical shift
pH

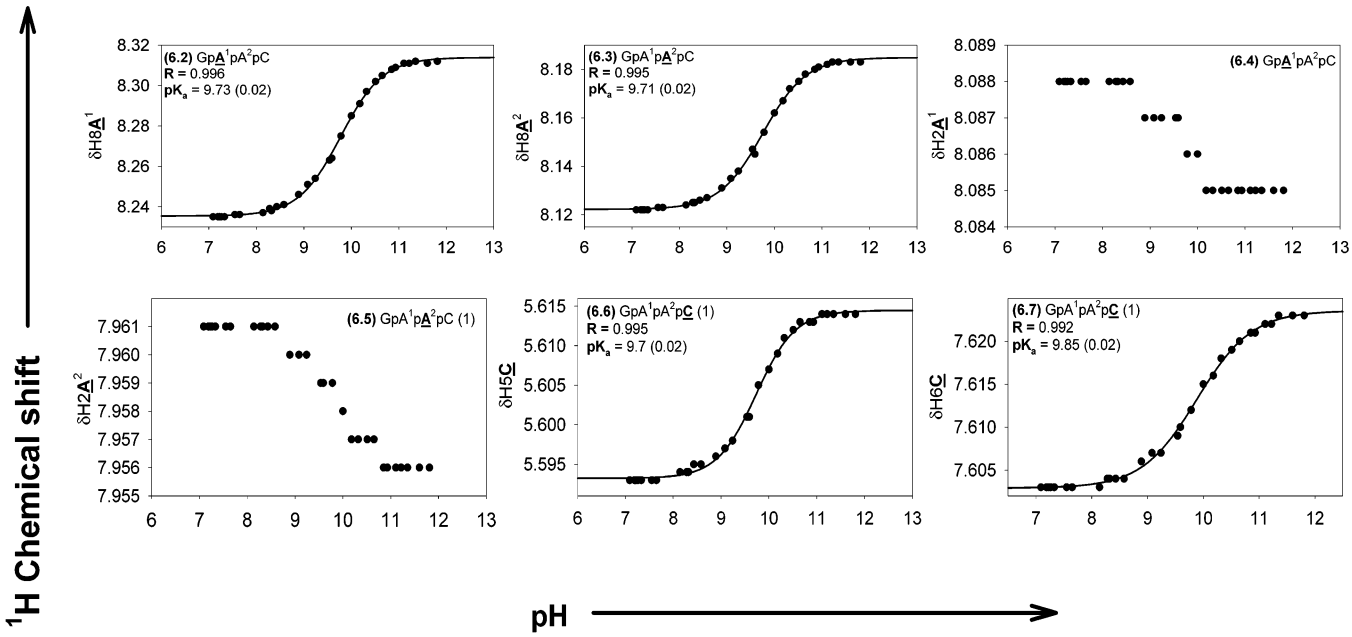

Figure 2. Plot of pH-dependent ($6.52 \leq$ pH ≤ 12.24) ^{1}H chemical shifts (δH) for different aromatic protons of oligomers **6**−**8** showing the pK_a at the inflection point. Chemical shift variations at 28−32 different pH values have been measured in an interval of 0.2−0.3 pH units to obtain the sigmoidal curves (see Experimental Section). Each graph shows chemical shift change with pH for one particular aromatic proton in a compound. The name of the compound along with the particular aromatic proton chosen for titration, the correlation coefficient *R* obtained from curve fitting, and the pK_a values obtained from the Hill plot analyses are shown in the respective graphs [see Experimental Section for details and Figure S2 in the Supporting Information]. Note that in all titration curves we have taken $\Delta\delta \approx 0.01$ ppm in order to calculate pK_a. Hence, pK_a values were not calculated for the marker protons corresponding to panels 8.4 (δH8**A**^{3} 0.001 ppm), 8.5 (δH8**A**^{4} 0.006 ppm), 8.8 (δH2**A**^{3} 0.004 ppm), 8.10 (δH5**C** 0.005 ppm), 7.8 (δH5**C** −0.005 ppm), 6.4 (δH2**A**^{1} 0.005 ppm), and 6.5 (δH2**A**^{2} 0.003 ppm) for which $\Delta\delta \approx 0.01$ ppm (see Figure 3).

or planar nucleobase rotation, thereby causing a destacking and destabilization of the ssRNA helix equilibrium as the pH becomes alkaline.

(i) pH Titration Studies. The pH titration studies[13e] with the GpA^{1}pA^{2}pA^{3}pA^{4}pC (**8**) showed (Figure 2, panels 8.1−8.11) the pK_a of N^1-H of guanin-9-yl (at the 5′-end) from its own δH8G (pK_a 9.76 ± 0.01) as well as from δH8A^1 (pK_a 9.65 ± 0.01) and δH2A^1 (pK_a 9.80 ± 0.01) of the p**A**^{1}p moiety, δH8A^2 (pK_a 9.95 ± 0.01) and δH2A^2 (pK_a 10.5 ± 0.07) of the p**A**^{2}p moiety, δH2A^4 (pK_a 9.66 ± 0.01) of the neighboring p**A**^{4}p moiety, and δH6C (pK_a 10.18 ± 0.03) of the terminal p**C**-3′ moiety.

No significant change in the pH-dependent shift of δH8A^3 ($\Delta\delta$ 0.001 ppm) and δH2A^3 ($\Delta\delta$ 0.004 ppm) of the p**A**^{3}p moiety was, however, found (Figure 2, panels 8.4 and 8.8), suggesting that there is an interruption of offset stacking with its two nearest neighbors, p**A**^{2}p and p**A**^{4}p. Similarly, δH8A^4 ($\Delta\delta$ 0.006 ppm) (but not δH2A^4) and δH5C ($\Delta\delta$ 0.005 ppm) (but not δH6C) also failed (Figure 2, panels 8.5 and 8.10) to show a titration plot, suggesting weak electrostatic interactions between electron densities of these atoms with those of the of nearest-neighbor nucleobases and phosphates.

A clear-cut assessment of the strength of these weak electrostatic interactions is difficult because of the following problems: (i) the chemical shift variation is *irregular* over the pH range, (ii) the $\Delta\delta$ values quoted above between two extreme pHs for H8A^4, δH8A^3, δH2A^3, and H5C of hexameric RNA in panels 8.4, 8.5, 8.8, and 8.10 are indeed very close to the experimental error (±0.001 ppm), (iii) if $\Delta\delta$ is obtained between extreme pHs, it can be seen that in panels 8.4, 8.5, 8.8, and 8.10 they are indeed 2-fold less than in panel 8.11 ($\Delta\delta$ 0.01 ppm). Note that in all titration curves we have taken $\Delta\delta \geq 0.01$ ppm in order to calculate pK_a. The possible reason for not observing a large and/or regular change of $\Delta\delta$ to give a pH titration curve for H8A^4, δH8A^3, δH2A^3, and H5C in **8** is that some of those edges or parts of the constituent nucleobases is/are relatively unstacked. Interestingly, p**A**^{3}p in **8** is perhaps fully bulged out since both its H8 and H2 remain nonresponsive over the pH range studied, although its %North (N) pseudorotamer population (see section D.iv and Figure 4) showed an increase of ∼13% over the pH range studied, which presumably suggests that the 9-adeninyl of p**A**^{3}p in the destacked state is taking up a relatively more pseudoaxial orientation.[11c] Thus, the edge(s) or part(s) of the nucleobase which might be more solvent exposed (such as H8A^4 or H5C) show larger electrostatic screening than the other edge(s) or part(s) (such as H2A^4 or H6C) of the nucleobases and, therefore, show only relatively weak electrostatic interaction with the negatively charged phosphates and the neighboring nucleobases.

The preferential atom−$\pi\sigma$ interactions,[5] which cause the electron densities of a specific atom (H8 over H2 in 9-adeninyl and H6 over H5 in 1-cytosinyl, see Figure 3) to interact with the nearest neighbor can also be seen through the observation of pK_a in the reference pentamer GpA^{1}pA^{2}pA^{3}pC (**7**) (panels 7.1−7.9) and tetramer GpA^{1}pA^{2}pC (**6**) (panels 6.1−6.7) in Figure 2, whereas the data for other reference compounds such as trimers,[4e] dimers,[4d] and monomers along with the oligo-RNAs **6**−**8** are summarized for comparison in Table 1.

(ii) Variation of pK_a among Different Marker Protons. Thus, the pK_a of 5′-**G**p residue from its own δH8G varies only slightly (from 9.76 ± 0.01 to 9.88 ± 0.01) in the oligo-RNAs **5**−**8**, which should be compared with the pK_a of 9.25 ± 0.02 for GpEt (**1a**), 9.17 ± 0.02 for GpA (**2a**), 9.56 ± 0.01 for GpC (**3a**), and 9.45 ± 0.02 for CpG (**3b**) as well as 9.57 ± 0.01 for 5′-EtpG (**1e**). The variation of pK_as for 5′-**G**p residue as

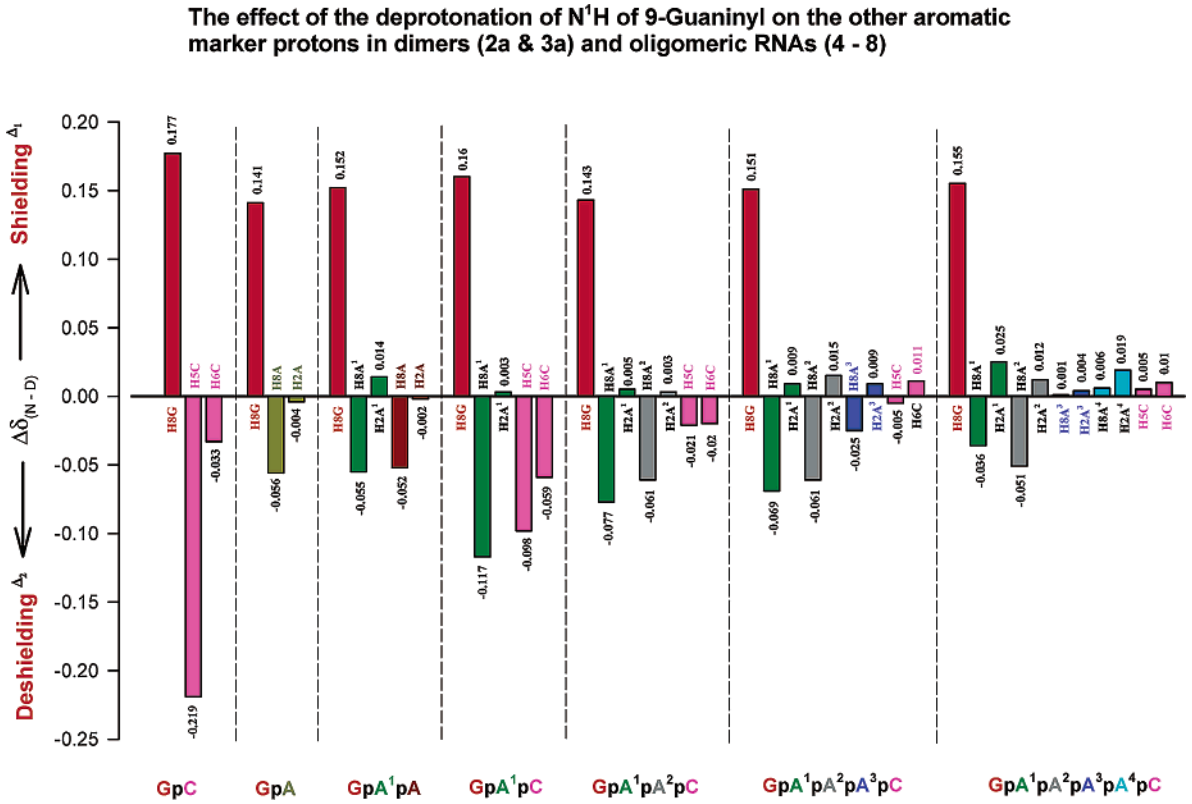

Figure 3. Effect of the N^1−H deprotonation of guanin-9-yl on the neighboring nucleobases (adenin-9-yl and cytosin-1-yl) for GpA (**2a**), GpC (**3a**), GpApA (**4**), GpApC (**5**), GpA^1pA^2pC (**6**), $GpA^1pA^2pA^3pC$ (**7**), and $GpA^1pA^2pA^3pA^4pC$ (**8**). The chemical shift differences [$\Delta\delta_{(N-D)}$, in ppm] between the neutral (N) and deprotonated (D) states have been plotted for all aromatic protons of all nucleotide residues in oligo-RNA **2**−**8** in order to show the competitive electrostatic interactions [atom−$\pi\sigma$ (present in both the N and D states) and relatively weaker anion(G^-)−π/dipole($Py^{\delta+}$) interactions (stabilizing) as well as anion(G^-)−π/dipole($Im^{\delta-}$) interaction (destabilizing)] [see section D.ii in the Results and Discussion for details]. It can be seen that as the chain length increases the free energy of stabilization of intramolecular stacking owing to atom−$\pi\sigma$ and relatively weaker anion(G^-)−π/dipole($Py^{\delta+}$) interactions[11] is opposing the anion(G^-)−π/dipole($Im^{\delta-}$) interaction (destabilizing) electrostatic interactions [compare the $\Delta\delta_{(N-D)}$ for all aromatic protons except for δH8G in the series of compounds **2a**−**8**]. Δ_1 Shielding signifies the relative upfield shift of a specific marker proton because of relatively more stacking with the neighbors as a result of deprotonation. Δ_2 Deshielding signifies the relative downfield shift of a specific marker proton because of relatively less stacking with the neighbors as a result of deprotonation.

measured from the other aromatic marker protons of various nucleotide residues in the hexameric RNA **8** is, however, more pronounced and varies from 9.65 ± 0.01 to 10.5 ± 0.07 along the RNA chain (Table 1, Figure 2). Table 1 shows, for comparison, that a similar variation of pK_as for 5′-**G**p residue from various marker protons is also found within the pentameric RNA **7** (9.59 ± 0.03 to 10.07 ± 0.03) (although it is much less for the tetrameric RNA **6** and almost negligible in trimeric RNA **5**). This variation of pK_as (ΔpK_a ± 0.9) of 9-guaninyl obtained from other nucleobases within the hexamer **8** represents a ΔG°_{pKa}[14a−c,f−i] difference ($\Delta\Delta G^\circ_{pKa}$) of ca. 5.1 kJ mol^{-1} (similarly, for pentamer **7**, ΔpK_a ± 0.48 corresponds to $\Delta\Delta G^\circ_{pKa}$ of 2.6 kJ mol^{-1}), which has been attributed to the variable strength of electrostatic interactions of the offset stacked nucleobases among themselves as well as with the phosphates.[4e] The net result of obtaining pK_as of a single ionization point (i.e., 9-guanylate ion) from different marker protons of neighboring nucleobase residue is that it allows us to experimentally examine the modulation of their respective electronic microenvironment along the ssRNA chain in a stepwise manner with considerable accuracy without having to make any assumptions. The chemical implication of this variable electrostatic interaction is that the microscopic change of the electronic environment around each constituent nucleobase along the RNA chain, even in a relatively small RNA molecule such as a pentamer or a hexamer, is not uniform. These differences should give rise to variable chemical reactivity along the ssRNA chain, as found for large biologically functional folded RNAs (partly hydrogen-bonded) that are involved in splicing,[13a,f] catalysis,[13a−d] or specific ligand binding by the aptamer.[17a]

(B) Accuracy of the pH-Dependent NMR Titration Studies. The pK_as reported here for the N^1 center of 9-guaninyl (obtained from δH8G as well as from other marker protons of neighboring residues) have been obtained by the Hill plot analysis of the pH-dependent ^{1}H chemical shifts measured by both 500 and 600 MHz NMR (see Supporting Information). The error in the chemical shift is ±0.001 ppm, and the error in pK_a determination is from ±0.01 to ±0.03, except for H2(p**A**^{4}p) in the hexamer **8** which is ±0.07 (all individual errors of respective pK_a values are shown in parentheses in Table 1 as well as in Figure 2). These accurate pK_a values and the resulting ΔG°_{pKa} values[14a−c,f−i] (error from ±0.1 to ±0.2) allow us to safely attribute the observed pK_a and ΔG°_{pKa} differences larger than ±0.05 and ±0.2, respectively, for various nucleotide residues [except for H2(p**A**^{4}p) in the hexamer **8**] to the differential intramolecular electrostatic interactions experienced by different pseudoaromatic nucleobases along the RNA chain. These differences in the electrostatic interactions can originate from either the phosphate and/or the neighboring nucleobases, which cannot be dissected in view of the fact that the addition of each nucleobase also involves the addition of one phosphate residue. However, the final outcome is the net pK_a change of

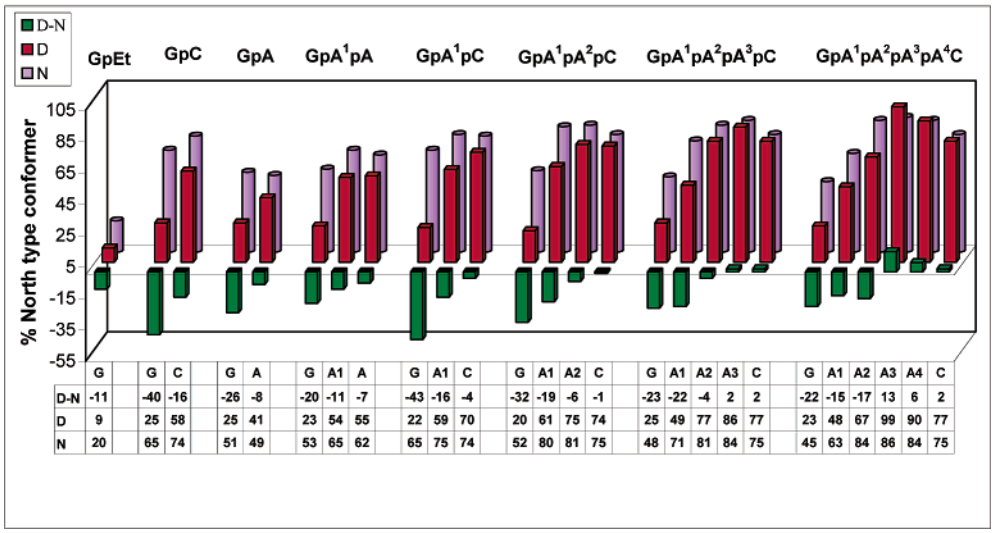

	G	G	C	G	A	G	A1	A	G	A1	C	G	A1	A2	C	G	A1	A2	A3	C	G	A1	A2	A3	A4	C
D-N	-11	-40	-16	-26	-8	-20	-11	-7	-43	-16	-4	-32	-19	-6	-1	-23	-22	-4	2	2	-22	-15	-17	13	6	2
D	9	25	58	25	41	23	54	55	22	59	70	20	61	75	74	25	49	77	86	77	23	48	67	99	90	77
N	20	65	74	51	49	53	65	62	65	75	74	52	80	81	75	48	71	81	84	75	45	63	84	86	84	75

Figure 4. Plot of the population of the North-type conformer [%North error ± 2.0%] of the 3′-*endo*-2′-*exo* (North-type) ⇆ 2′-*endo*-3′-*exo* (South-type) pseudorotational equilibrium[12] of the respective pentofuranose moiety in each nucleotidic unit in GpEt (**1a**), GpA (**2a**), GpC (**3a**), GpApC (**5**), GpA^{1}pA^{2}pC (**6**), GpA^{1}pA^{2}pA^{3}pC (**7**), and GpA^{1}pA^{2}pA^{3}pA^{4}pC (**8**) at the neutral (N, shown in violet bar) and deprotonated (D, shown in red bar) states (see the table below the plot for %North-type population values at N and D states as well as the difference between these two states, i.e., D−N). The bars are in the same order as the sequence starting from 5′-Gp on the left. The $^3J_{1'2'}$ values are shown in the Supporting Information. The difference between the D and the N states (D−N, shown in green bar) shows the relative stacking (increase of %North-type) or destacking (decrease of %North-type) over the pH-titration range. It can be seen from D−N values that, upon generation of the 5′-guanylate ion, the destacking takes place until the third nucleotide in the hexamer, whereas it proceeds up to the second nucleotide in the tetra- and pentamer (compare with the more sensitive $\Delta\delta_{(N-D)}$ values in Figure 3).

9-guaninyl moiety observed from δH8G as well as the pK_a modulation of 5′-**G**p residue observed from other marker protons of the neighboring nucleobases in the series of oligomeric RNAs **2**−**8**, which gives us a measure of variable pseudoaromaticity (and chemical reactivity) along the chain of a ssRNA molecule.

(C) Tandem Electrostatic Interaction Is a Result of the Electronic Coupling of the Neighboring Nucleobases and the Phosphates. *(i) Different pK_a Shift of Nucleobases due to Variable Electrostatic Effects of 3′- versus 5′-Phosphate.* Comparison of the pK_a of 9-guaninyl in GpEt (**1a**) (9.25 ± 0.02)[4d] and EtpG (**1e**) (9.57 ± 0.01) shows (Table 1) that the 5′-phosphate in the latter makes the pK_a of 9-guaninyl more basic compared to the 3′-phosphate in the former. This is simply because of the fact that the spatial proximity of the 5′-phosphate and the imidazole moiety of the 9-guaninyl (in the anti conformation) in EtpG produces an effective electrostatic repulsion of their electron clouds, which enhances the electron density in the fused pyrimidine moiety, giving an overall increase of pK_a of 9-guaninyl in EtpG (**1e**) compared to that of GpEt (**1a**). It is, therefore, likely that the relative spatial orientation of the phosphates vs nucleobases may have a critical role in steering the pK_a and hence the chemical reactivity of purine nucleobases in ssRNA.

(ii) Different pK_a Shift of Nucleobases due to Nearest-Neighbor Electrostatic Effect. The pairwise comparison at the dimer level, however, shows (Table 1) that the pK_a of N^1-H of 9-gunaniyl residue in the **Gp**A (**2a**)[4d] (9.17 ± 0.02)/**Gp**C (**3a**) (9.56 ± 0.01) (ΔpK_a ± 0.41) is sequence dependent since the two isomeric dimers have the same phosphate charge but different 3′-nucleobase. Even at the trimer level,[4e] the comparison of **Gp**ApA (**4**) and **Gp**ApC (**5**) shows that although they have the same phosphate charge there is a slight difference in the pK_a of the 9-guaninyl residue (ΔpK_a ± 0.13, which is well above the error limit, Table 1). This suggests that the chemical nature of the nucleobase steers the pK_a of the nearest-neighbor nucleobase(s) more effectively than the phosphates.

(15) (a) *Comparison of δ among Dimers:* The effect of anionic guanin-9-yl decreases (decreasing $\Delta\delta$ from the trimer to hexamer), in general, with increasing chain length of oligonucleotide (Table 2). Interestingly, a simple comparison of $\Delta\delta_{(N-D)}$ for H8G of 9-guaninyl in **G**pC (pK_a 9.57) and **G**pA (pK_a 9.17) shows (Figure 3) how the nearest neighbor (p**C** vs p**A**) modulates the pseudoaromaticity of the 9-guaninyl in the neutral (δH8G: 8.039 for GpC and 7.906 for GpA) and anionic form (δH8G: 7.862 for GpC and 7.765 for GpA). (b) *Comparison of δ among Trimers to Hexamer:* Comparison of $\Delta\delta_{(N-D)}$ for pA^{1}p in GpA^{1}pA and GpA^{1}pA^{2}pC shows the effect of 3′-terminal 1-cytosinyl of pC on the electronic makeup of pA^{1}p. Similar comparison of $\Delta\delta_{(N-D)}$ for p**A**^{1}p in GpA^{1}pA and GpA^{1}pC shows the effect of the nearest neighbor at 3′-end (p**C** vs p**A**) on the chemical environment of p**A**^{1}p. A comparison of $\Delta\delta_{(N-D)}$ for p**A**^{1}p and p**A**^{2}p also shows that the relative effect of anionic 9-guaninyl remains to be almost the same in tetramer (GpA^{1}pA^{2}pC) and pentamer (GpA^{1}pA^{2}pA^{3}pC) relative to the trimers GpA^{1}pA (**4**) and GpApC (**5**). The effect of 9-guanylate ion is considerably reduced in the hexamer **8**. This is because the intramolecular offset stacking through atom−$\pi\sigma$ interaction that opposes the anion−π/dipole interaction is strongest in the hexamer **8** in our series of oligomers studied, which is evidenced by a relatively much smaller change in chemical shifts [$\Delta\delta_{(N-D)}$] of all marker protons of all neighboring nucleobases in the former compared to the latter (Figure 3). This means that the electrostatic interaction of 9-guanylate ion with the neighboring nucleobases tends to be minimal after the p**A**^{2}p moiety in the hexamer (clearly detectable up to p**A**^{3}p in pentamer **7** in comparison with the hexamer **8**, Figure 3). This also means that the pseudoaromaticity of the triplet codon, independent of the RNA chain length, is maximally cross-modulated owing to their full electronic coupling with the nearest neighbor. Clearly, the last three nucleobases at the 3′-end of the hexamer **8** are sensing the electrostatic interaction owing to the anionic character of 9-guaninyl moiety to a much lesser extent (ca. 10−15%) compared to the first two nucleobases after 5′-Gp anion. This is because of the fact that the attractive Coulombic forces stabilize the stacked state of the hexamer more efficiently than in the pentamer. As a result, this stabilizing atom−$\pi\sigma$ interaction counteracts the destabilizing anion−π interaction more efficiently in the former than in the latter.

(16) (a) For review, see: Patel, D. J.; Suri, A. K. *Rev. Mol. Biotechnol.* **2000**, *74*, 39. (b) Consonni, R.; Arosio, I.; Belloni, B.; Fogolari, F.; Fusi, P.; Shehi, E.; Zetta, L. *Biochemistry* **2003**, *42*, 1421. (c) Fogolari, F.; Ragona, L.; Licciardi, S.; Romagnoli, S.; Michelutti, R.; Ugolini, R.; Molinari, H. *Proteins: Struct., Funct., Genet.* **2000**, *39*, 317.

(17) For review, see: Ramakrishnan, V. *Cell* **2002**, *69*, 557.

Table 1. pK_a[a] and ΔG°_{pKa}[b] of the 9-Guanylate Ion in Mono- and Oligo-RNAs **1**−**8**

Compounds		pK$_a$ and $\Delta G^\circ_{pK_a}$ of 9-guanylate ion in mono- and oligo-RNAs[a,b]					
		δH8			δH2 / δH5 / δH6		
		pK$_a$	$\Delta G^\circ_{pK_a}$	$\Delta\Delta G^\circ_{pK_a}$	pK$_a$	$\Delta G^\circ_{pK_a}$	$\Delta\Delta G^\circ_{pK_a}$
GpEt (**1a**)[c]		9.25 (± 0.02)	**52.8 (± 0.1)**	-	-	-	-
3′-**G**MP (**1b**)		9.33 (± 0.01)	**53.2 (± 0.1)**	-	-	-	-
5′-**G**MP (**1c**)		9.74 (± 0.01)	**55.6 (± 0.1)**	-	-	-	-
Etp**G**pEt (**1d**)		9.57 (± 0.01)	**54.6 (± 0.1)**	-	-	-	-
5′-Etp**G** (**1e**)		9.57 (± 0.01)	**54.6 (± 0.1)**	-	-	-	-
GpA (**2a**)[c]	**G**p	9.17 (± 0.02)	**52.4 (± 0.1)**	*-0.4*	-	-	-
	p**A**	9.11 (± 0.02)	**52.0 (± 0.1)**	*-0.8*	-[d]	-[d]	-[d]
Ap**G** (**2b**)[c]	A**p**	9.71 (± 0.01)	**55.4 (± 0.1)**	*0.8*	9.65 (± 0.01)	**55.1 (± 0.1)**	*0.5*
	p**G**	9.42 (± 0.01)	**53.7 (± 0.1)**	*-1.1*	-	-	-
GpC (**3a**)	**G**p	9.56 (± 0.01)	**54.5 (± 0.1)**	*1.7*			
	p**C**	-	-	-	9.56 (± 0.01)[e] 9.51 (± 0.01)[f]	**54.5 (± 0.1)** **54.3 (± 0.1)**	*1.7* *1.5*
Cp**G** (**3b**)	C**p**	-	-	-	9.42 (± 0.02)[e] 9.42 (± 0.02)[f]	**53.7 (± 0.1)** **53.7 (± 0.1)**	*-0.9* *-0.9*
	p**G**	9.45 (± 0.02)	**53.9 (± 0.1)**	*-0.7*	-	-	-
GpApA (**4**)[c]	**G**p	9.75 (± 0.02)	**55.6 (± 0.1)**	*2.8*	-	-	-
	pA**p**	9.74 (± 0.02)	**55.6 (± 0.1)**	*2.8*	9.82 (± 0.02)	**56.0 (± 0.1)**	*3.2*
	p**A**	9.78 (± 0.02)	**55.8 (± 0.1)**	*3.0*	-[d]	-[d]	-[d]
GpApC (**5**)[c]	**G**p	9.88 (± 0.02)	**56.4 (± 0.1)**	*3.6*	-	-	-
	pA**p**	9.88 (± 0.02)	**56.4 (± 0.1)**	*3.6*	-[d]	-[d]	-[d]
	p**C**	-	-	-	9.89 (± 0.02)[e] 9.90 (± 0.02)[f]	**56.4 (± 0.1)**[e] **56.5 (± 0.1)**[f]	*3.6* *3.7*
GpA^{1}pA^{2}pC (**6**)	**G**p	9.76 (± 0.01)	**55.7 (± 0.1)**	*2.9*	-	-	-
	pA^1**p**	9.73 (± 0.02)	**55.5 (± 0.1)**	*2.7*	-[d]	-[d]	-[d]
	pA^2**p**	9.71 (± 0.02)	**55.4 (± 0.1)**	*2.6*	-[d]	-[d]	-[d]
	p**C**	-	-	-	9.70 (± 0.02)[e] 9.85 (± 0.02)[f]	**55.3 (± 0.1)**[e] **56.2 (± 0.1)**[f]	*2.5* *3.4*
GpA^{1}pA^{2}pA^{3}C (**7**)	**G**p	9.82 (± 0.01)	**56.0 (± 0.1)**	*3.2*	-	-	-
	pA^1**p**	9.73 (± 0.01)	**55.5 (± 0.1)**	*2.7*	9.78 (± 0.03)	**55.8 (± 0.1)**	*3.0*
	pA^2**p**	9.76 (± 0.01)	**55.7 (± 0.1)**	*2.9*	10.07 (± 0.04)	**57.5 (± 0.2)**	*4.7*
	pA^3**p**	9.68 (± 0.03)	**55.2 (± 0.2)**	*2.4*	9.59 (± 0.03)	**54.7 (± 0.2)**	*1.9*
	p**C**	-	-	-	-[d,e] 9.63 (± 0.03)[d]	-[d,e] **54.9 (± 0.2)**[f]	-[d,e] *2.1*
GpA^{1}pA^{2}pA^{3}A^{4}pC (**8**)	**G**p	9.76 (± 0.01)	**55.7 (± 0.1)**	*2.9*	-	-	-
	pA^1**p**	9.65 (± 0.01)	**55.1 (± 0.1)**	*2.3*	9.80 (± 0.01)	**55.9 (± 0.1)**	*3.1*
	pA^2**p**	9.95 (± 0.01)	**56.8 (± 0.1)**	*4.0*	10.50 (± 0.07)	**59.9 (± 0.4)**	*7.1*
	pA^3**p**	-[d]	-[d]	-[d]	-[d]	-[d]	-[d]
	pA^4**p**	-[d]	-[d]	-[d]	9.66 (± 0.01)	**55.1 (± 0.1)**	*2.3*
	p**C**	-	-	-	-[d,e] 10.18 (± 0.03)[f]	-[d,e] **58.1 (± 0.2)**[f]	-[d] *5.3*

[a] All pK_a values and their corresponding errors have been calculated from Hill plot analyses (See Figure 1 for the titration plots and Figure S2 in the Supporting Information for details of Hill plot analyses). [b] The free energy of deprotonation (ΔG°_{pKa}, in kJ mol^{-1}) of guanin-9-yl for compounds **1**−**8** has been calculated using the equation[14a−c,f−i] $\Delta G^\circ_{pKa} = 2.303RTpK_a$. Similarly, $\Delta\Delta G^\circ_{pKa}$ (in kJ mol^{-1}) values have been calculated using relation $\Delta\Delta G^\circ_{pKa} = 2.303RT\Delta pK_a$ where $\Delta pK_a = [pK_a]_{\text{obtained from each residue}} - [pK_a]_{\mathbf{1a}\text{ and/or }\mathbf{1e}}$. [c] Data have been taken from refs 4d,e. [d] No titration plot observed. The chemical shift difference over the pH range [$\Delta\delta_{N-D}$, in ppm] was much closer to the error limit (see Figures 2 and 3). Thus, no pK_a, ΔG°_{pKa}, and $\Delta\Delta G^\circ_{pKa}$ have been calculated. [e] For δH5C. [f] For δH6C.

(iii) Comparison of ΔG°_{pKa} of Different Marker Protons Shows Different Pseudoaromatic Character of the Neighboring Nucleobases. The $\Delta G^{\circ\ 14a-c,f-i}_{pKa}$ for 9-guaninyl from different aromatic marker protons of the neighboring nucleobases varies (Table 1) from 55.6 ± 0.1 to 56.0 ± 0.1 kJ mol^{-1} for **G**$^-$pApA (**4**),[4e] 56.4 ± 0.1 kJ mol^{-1} for **G**$^-$pApC (**5**),[4e] 55.3 ± 0.1 to 56.2 ± 0.1 kJ mol^{-1} for **G**$^-$pApApC (**6**), 54.7 ± 0.2 to 57.5 ± 0.2 kJ mol^{-1} for **G**$^-$pApApApC (**7**), and 55.1 ± 0.1 to 59.9 ± 0.7 kJ mol^{-1} for **G**$^-$pApApApApC (**8**). These values should be compared with the ΔG°_{pKa} of 52.8 ± 0.1 kJ mol^{-1} for G$^-$pEt (**1a**),[4d] 52.4 ± 0.1 kJ mol^{-1} for G$^-$pA (**2a**),[4d] and 53.9 ± 0.1 kJ mol^{-1} for of CpG$^-$ (**3b**).

The ΔG°_{pKa} for 9-guaninyl obtained from any other marker protons (H8A/H2A or H5/H6C) of the neighboring nucleobases within any single oligo-RNA **2a**−**8** (52−59.9 kJ mol^{-1}) is variable in a sequence-specific manner owing to different electronic coupling between any two next neighbors (Table 1). The lowering of the pK_a value obtained from a given marker proton (i.e., from δH8A, δH2A, or δH5/H6C) of a nucleobase relative to 9-guaninyl (i.e., from δH8G) in a given oligo-RNA suggests a higher electrostatic screening. On the other hand, an increase of the pK_a value found from a marker proton of a nucleobase relative to 9-guaninyl in a given oligo-RNA suggests an added electronic contribution from those nucleobases themselves owing to their specific pseudoaromatic character orchestrated by the change of the local microenvironment.

The differences in $\Delta G^{\circ\ 14a-c,f-i}_{pKa}$ from 9-guaninyl with respect to the monomeric GpEt (**1a**) or 5′-EtpG (**1e**) (i.e., $\Delta\Delta G^\circ_{pKa}$) is a measure of the relative stability of the 9-guanylate ion in the stacked vs destacked state (Table 1) owing to

variable efficiency of the electrostatic interactions (from −1.1 to 3.6 kJ mol^{-1} in **2a**−**8**). On the other hand, the ΔG°_{pKa} for 9-guaninyl from the marker protons of other nucleobases show the subsequent electrostatic modulation ($\Delta\Delta G^{\circ}_{pKa} \approx -0.9$ to 7.1 kJ mol^{-1}), depending upon the sequence context as well as the number of phosphates (chain length) of the oligo-RNA chain. The ΔG°_{pKa} is always larger ($\Delta\Delta G^{\circ}_{pKa} > 0$) in all residues of oligo-RNA than the monomeric GpEt (**1a**) (Table 1) with the exception of GpA (**2a**)[4d] as well as for p**G** of ApG (**2b**) and CpG (**3b**).

The fact that the pK_a (Table 1) of 5′-**G**p residue can be measured from its own marker proton as well as from the other marker protons of the neighboring residues in ssRNA shows that the constituent nucleobases in the hexamer **8** (in which the first to sixth nucleotide residue is ∼21Å apart in the unfolded state), as well as in the dimers, trimers, tetramer, and pentamer **2a**−**7**, are electronically coupled because of the offset stacking. This enables each nucleobase in the chain to engage with the next neighbor(s) through a variable electrostatic interaction, depending upon their individual pseudoaromatic characters modulated by their respective microenvironments.[4e]

(D) Mechanism of Interplay of Electrostatic Interactions in ssRNA. The aromatic interactions[5−9] involved among the nearest-neighbor nucleobases in our oligo-RNA system are more complex in nature compared to that observed in nonbiological molecules[5−7] containing simple aryl systems such as phenyl[6e,f] or naphthyl.[6g] The attractive atom−$\pi\sigma$ interaction[5] in the offset stacked geometry exists among the neutral 9-guaninyl and neighboring 9-adeninyl, between 9-adeninyl and 9-adeninyl, as well as between 9-adeninyl and 1-cytosinyl (3′-end) in the tetrameric, pentameric, and hexameric RNAs, as originally observed by us for the dimeric[4d] and trimeric[4e] RNAs.

(i) Participants in the Electrostatic Cross-Modulation in RNA. Under quasiphysiological conditions, we have an electrostatic interplay between different electron clouds of various pseudoaromatic nucleobases which are modulated by the phosphate and the 2′-OH. In contrast, the electronic factors that contribute to the microenvironmental changes in our oligo-RNAs under alkaline pH are the mutual interactions and interplay of four electron-rich partners: (i) phosphates, (ii) the vicinal 2′-OH (free or intra- or intermolecularly hydrogen-bonded), (iii) guanylate ion, and (iv) different pseudoaromatic nucleobases.

Clearly, the observed ΔG°_{pKa} from each marker proton in our ssRNA has, however, two contributors: (1) the electronic contribution from the specific pseudoaromatic character of each nucleobase (Q) (i.e., their relative electron-rich or electron-deficient character, $[\Delta G^{\circ}_{pKa}]_{(\text{marker proton of Q})} - [\Delta G^{\circ}_{pKa}]_{(\text{H8G from the ssRNA})}$, and (2) the ΔG°_{pKa} of 9-guaninyl itself (**Type 1** effect,[4e] which is $[\Delta G^{\circ}_{pKa}]_{(H8G)}$. These two contributing terms [(1) + (2)] together define the specific free-energy difference (**Type 2** effect[4e]) of the two-state protonation ⇆ deprotonation equilibrium of 9-gunainyl, which is observed in each of the *other* aromatic marker protons in the RNA molecule. Hence, the number of ΔG°_{pKa} can be as high as the number of marker protons available in an oligo-RNA because of their different chemical nature and also depending upon how the edges of the nucleobases sense the immediate chemical microenvironment around them. This variation of immediate chemical microenvironment modulates (polarize) the electron distribution of the offset stacked nucleobases, which is manifested in the observed variation pK_as of 9-guaninyl from different marker protons within the hexamer (Δp$K_a \pm 0.9$, $\Delta\Delta G^{\circ}_{pKa} \approx 5.1$ kJ mol^{-1}) and pentamer (Δp$K_a \pm 0.48$, $\Delta\Delta G^{\circ}_{pKa} \approx 2.6$ kJ mol^{-1}).

(ii) Origin of Atom−$\pi\sigma$ and Anion(G$^-$)-Purine−π/Dipole Interactions. We considered both atom−$\pi\sigma$[5] and the anion-(G$^-$)−purine-π/dipole interactions in order to explain the observed electrostatic interaction[4f,9] for tetrameric, pentameric, and hexameric RNAs across the pH range of 7−12. The interaction between the 9-guanylate ion and the neighboring 9-adeninyl system is complex because of the fact that a 9-adeninyl moiety, consisting of electron-rich imidazole (Im$^{\delta-}$) fused with the electron-deficient pyrimidine (Py$^{\delta+}$) system, has a permanent dipole (π/dipole) ($\mu \pm 3.0-3.7$ D).[14d] This means that the electrostatic interaction between the neighboring 9-guanylate ion and 9-adeninyl can either be *repulsive* anion(G$^-$)−π/dipole(Im$^{\delta-}$) or *attractive* anion(G$^-$)−π/dipole(Py$^{\delta+}$) interaction, depending upon their relative orientation. The relative chemical shift differences [$\Delta\delta_{(N-D)}$] of protons of various nucleotide residues in the oligo-RNAs between the neutral (N) and the deprotonated (D) states of 5′-Gp residue here show (Figure 3) (i) how far the electrostatic anion(G$^-$)−π/dipole-(Im$^{\delta-}$) interactions propagate along the RNA chain and (ii) how the interplay of the stabilizing atom−$\pi\sigma$ and anion(G$^-$)−π/dipole(Py$^{\delta+}$) interactions vs the destabilizing anion(G$^-$)−π/dipole(Im$^{\delta-}$) interaction dictate the two-state stacking ⇆ destacking equilibria as a function of pH[13e] along the RNA chain. In this connection, it should be emphasized that the δH8 (marker for the imidazole part of the 9-adeninyl) suffers larger deshielding upon deprotonation because of destacking owing to repulsive anion(G$^-$)−π/dipole(Im$^{\delta-}$) interactions, whereas δH2 (marker for the pyrimidine part of the 9-adeninyl) shows only shielding in the D state because of the attractive anion-(G$^-$)−π/dipole(Py$^{\delta+}$) interaction.

(iii) Effect of Atom−$\pi\sigma$ and Anion(G$^-$)−Purine-π/Dipole Interactions. The implication of generating a negatively charged center, upon N^1 deprotonation of 9-guaninyl residue, is that the nucleobases in the ssRNA chain become partially electronically decoupled (destacked), which is evidenced by the destablization of the helix, compared to that in the neutral state (Figure 3). Comparison of the relative δH8 shift (Table 2) as well as the relative magnitude of $\Delta\delta_{(N-D)}$ of all aromatic protons in Figure 3, however, shows that the extent of this electrostatic promoted decoupling/destacking within the ssRNA helix is distance-dependent. This demonstrates that the effect of 9-guanylate charge at the 5′-terminus is perhaps largest until the third nucleobase, and then this effect is felt less and less as the distance between this charge and a given nucleobase increases in the helix.

As the pH becomes alkaline, the phosphate being negatively charged should repel the negatively charged guanylate anion. The alignment of all other nucleobases in the RNA sequence should be dictated by the guanylate−phosphate repulsion, which will be further modulated in a variable manner depending upon the individual pseudoaromatic character of the nucleobases. This may initiate a new stacking orientation and/or planar nucleobase rotation, which would steer the two-state stacking ⇆ destacking equilibria to a relatively more destacked state, causing a destabilization of the ssRNA helix. This destablization of the

Table 2. ^{1}H Chemical Shifts [δ_H, in ppm][a] at the Neutral (N) and the Deprotonated (D)[a] States at 298 K for Compounds **1**−**8**

compounds		δ_{H8}		δ_{H2}		δ_{H6}		δ_{H5}	
		N	D	N	D	N	D	N	D
GpEt (**1a**)[b]		8.010	*7.861*						
Etp**G**pEt (**1d**)		8.097	*8.011*						
5-Etp**G** (**1e**)		8.078	*7.976*						
Etp**A**pEt (**1f**)		8.493	*8.493*	8.284	*8.283*				
5′-Etp**C** (**1g**)						7.934	*7.933*	6.100	*6.099*
GpA (**2a**)[b]	**G**p	7.906	*7.765*						
	p**A**	8.345	*8.401*	8.206	*8.210*				
GpC (**3a**)	**G**p	8.039	*7.862*						
	p**C**					7.821	*7.854*	5.704	*5.923*
CpG (**3b**)	**C**p					7.743	*7.640*	5.589	*5.789*
	p**G**	8.036	*7.975*						
GpA^{1}pA (**4**)[b]	**G**p	7.903	*7.751*						
	p**A**^{1}p	8.234	*8.289*	8.133	*8.119*				
	p**A**	8.225	*8.277*	8.024	*8.022*				
GpApC (**5**)[b]	**G**p	7.958	*7.798*						
	p**A**p	8.278	*8.395*	8.163	*8.160*				
	p**C**					7.668	*7.737*	5.658	*5.756*
GpA^{1}pA^{2}pC (**6**)	**G**p	7.922	*7.779*						
	p**A**^{1}p	8.235	*8.312*	7.961	*7.956*				
	p**A**^{2}p	8.122	*8.183*	8.088	*8.085*				
	p**C**					7.603	*7.623*	5.593	*5.614*
GpA^{1}pA^{2}pA^{3}C (**7**)	**G**p	7.887	*7.736*						
	p**A**^{1}p	8.216	*8.285*	7.907	*7.898*				
	p**A**^{2}p	8.084	*8.145*	7.878	*7.863*				
	p**A**^{3}p	8.029	*8.054*	8.054	*8.045*				
	p**C**					7.573	*7.562*	5.530	*5.535*
GpA^{1}pA^{2}pA^{3}p A^{4}C (**8**)	**G**p	7.875	*7.720*						
	p**A**^{1}p	8.206	*8.242*	7.905	*7.880*				
	p**A**^{2}p	8.091	*8.142*	7.817	*7.805*				
	p**A**^{3}p	8.000	*7.999*	8.058	*8.052*				
	p**A**^{4}p	7.969	*7.963*	7.827	*7.808*				
	p**C**					7.558	*7.543*	5.508	*5.503*

[a] The chemical shifts at the deprotonated (D) state are given in italics. All chemical shifts are measured with respect to internal standard DSS (δ_{DSS} = 0.015 ppm). See the Experimental Section for details. [b] Data are taken from refs 4d,e.

helix dictates a change of relative shielding or deshielding of a specific marker proton owing to the reorientation of the stacking geometry of the nearest neighbor(s). This may be the reason when H8A becomes deshielded, H2A responds by slight shielding by simple syn ⇆ anti shift of the glycosyl torsion. Clearly, in the absence of the vicinal 3-bond coupling constant data for the torsional angles of the sugar−phosphate backbone or the dipolar coupling data for deriving the relative orientation of the RNA molecule at the neutral versus deprotonated state, it is simply not possible to differentiate this pH-dependent geometrical change in any exact terms.

(iv) Destabilization of ssRNA Helix in Alkaline pH Has Two Indicators: More Positive $\Delta G^\circ_{North/South(298K)}$ *and Relative Deshielding of H8A.* It is well-known[1a] that in stacked helical oligo-RNA (i) the overall conformation of the sugar moieties is 3′-*endo*-2′-*exo* (North-type) because this allows nucleobases to be pseudoaxial,[11c] thereby bringing them in closer spatial proximity (3−3.5 Å) to be electronically coupled[4d,e] with the nearest neighbor, and (ii) the aromatic ring current of a given heterocycle has a shielding effect on the protons of the adjacent stacked heterocycle. Upon destabilization[4d,e,13b−d] of stacking in oligo-RNA, the reversal of this process has been found to take place in a dynamic manner[11c] in that an increase of the South(S)-type pseudorotamer population over the North(N)-type as well as a deshielding of the aromatic protons are observed. In a similar manner, concurrent with the deshielding of H8A proton in the alkaline pH compared to the neutral counterpart, we also observe a shift of the 3′-*endo*-2′-*exo* (North-type) ⇆ 2′-*endo*-3′-*exo* (South-type) equlibrium [$\Delta G^\circ_{North/South(298K)}$][11c] of individual sugar units (see Figures 4 and 5) to the more South-type conformation in the deprotonated oligo-RNAs, thereby confirming that the destabilization of the stacked RNA helix indeed takes place in alkaline pH as a result of the guanylate ion formation.

Hence, in the case of pentameric and hexameric RNA, it is correct to say that the H8A deshielding in the alkaline pH is synonymous of the lost stability of stacking as evident from the $\Delta G^\circ_{North/South(298K)}$ shift in favor of the S-type conformation.

The $\Delta\Delta G^\circ_{D-N(298K)}$ values in Figure 5 also show that the destacking takes place more efficiently up to the third nucleotidic residue (from the 5′-end), and then it gradually decreases from the pA^{3}p to pC-3′ in GpA^{1}pA^{2}pA^{3}pC (**7**) and pA^{4}p to pC-3′ in GpA^{1}pA^{2}pA^{3}pA^{4}pC (**8**).

(v) Why Does the Destacking in Alkaline pH Become Less and Less Prominent as the ssRNA Chain Length Increases? The strength of the stacking in ssRNA increases as the chain length increases, and hence, the δH8/H2 of 9-adeninyl and δH5/H6 of 1-cytosinyl moieties are more shielded in oligo-RNAs **2**−**8** (Table 2) in the N state, just as the H8G, compared to their monomeric counterpart.[15b] On the other hand, the $\Delta\delta_{(N-D)}$ shows that the relative shielding of H8/H2A as well as H5/6C protons (with much less pronounced change for H8G) in the D state becomes less and less as the chain length increases as a result of a shift of the two-state stacking ⇆ destacking equilibrium[11c,13e] toward a destacked state (predominantly up to third nucleobase). Thus, the relative $\Delta\delta_{(N-D)}$ for all aromatic marker protons except H8G (Figure 3) decreases in the following order: GpC < GpApC < GpApApC < GpApApApC < GpApApApApC.

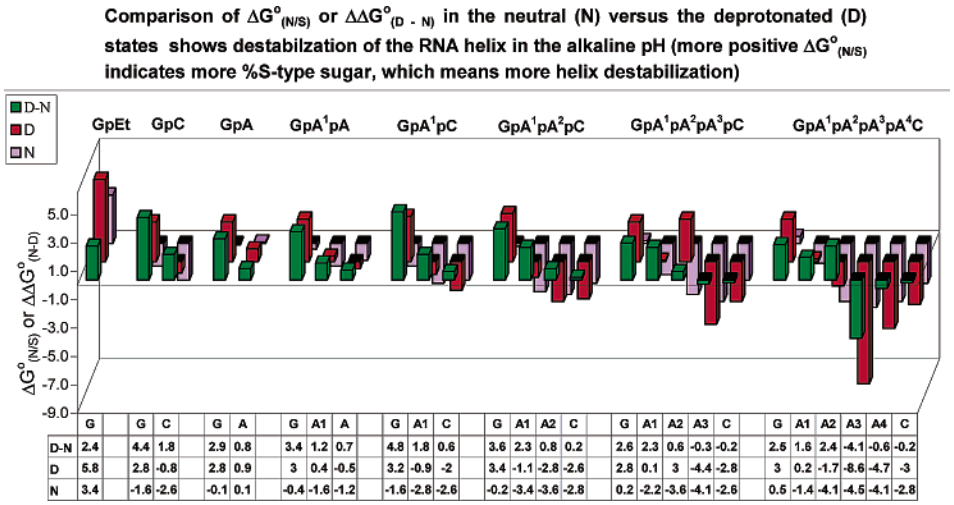

	G		G	C		G	A		G	A1	A		G	A1	C		G	A1	A2	C		G	A1	A2	A3	C		G	A1	A2	A3	A4	C
D-N	2.4		4.4	1.8		2.9	0.8		3.4	1.2	0.7		4.8	1.8	0.6		3.6	2.3	0.8	0.2		2.6	2.3	0.6	-0.3	-0.2		2.5	1.6	2.4	-4.1	-0.6	-0.2
D	5.8		2.8	-0.8		2.8	0.9		3	0.4	-0.5		3.2	-0.9	-2		3.4	-1.1	-2.8	-2.6		2.8	0.1	3	-4.4	-2.8		3	0.2	-1.7	-8.6	-4.7	-3
N	3.4		-1.6	-2.6		-0.1	0.1		-0.4	-1.6	-1.2		-1.6	-2.8	-2.6		-0.2	-3.4	-3.6	-2.8		0.2	-2.2	-3.6	-4.1	-2.6		0.5	-1.4	-4.1	-4.5	-4.1	-2.8

Figure 5. Free energy [$\Delta G^{\circ}_{\text{North/South(298K)}}$ in kJ mol^{-1} represented in the figure as $\Delta G^{\circ}_{\text{N/S}}$] estimations for the 3′-*endo*-2′-*exo* (North-type) ⇆ 2′-*endo*-3′-*exo* (South-type) pseudorotational equilibrium[12] for the respective pentofuranose moiety in each nucleotidic unit in GpEt (**1a**), GpA (**2a**), GpC (**3a**), GpApC (**5**), GpA^{1}pA^{2}pC (**6**), GpA^{1}pA^{2}pA^{3}pC (**7**), and GpA^{1}pA^{2}pA^{3}pA^{4}pC (**8**) at the neutral (N, shown in violet bar) and deprotonated (D, shown in red bar) states (see the table below the plot for $\Delta G^{\circ}_{\text{North/South(298K)}}$ values at N and D states as well as the difference between these two states, i.e., D−N). The free-energy values have been calculated using Gibbs relation: $\Delta G^{\circ}_{\text{North/South(298K)}} = -RT \ln K$, where $K = (x_N/x_S)$ and $T = 298$ K (See the Experimental Section and Figure 4 for details of the thermodynamic calculations). $\Delta\Delta G^{\circ}_{\text{D−N(298K)}}$ values have been calculated using the relation $[\Delta G^{\circ}_{\text{North/South(298K)}}]_D - [\Delta G^{\circ}_{\text{North/South(298K)}}]_N = \Delta\Delta G^{\circ}_{\text{D−N(298K)}}$. The bars are in the same order as the sequence starting from 5′-Gp on the left. The difference between the D and the N states (D−N, shown in green) shows the relative stacking (negative free energy) or destacking (positive free energy) over the pH-titration range. It can be seen from D−N values that, upon generation of the 5′-guanylate ion, the destacking takes place until the third nucleotide in the hexa-, tetra-, and pentamer (compare with the more sensitive $\Delta\delta_{(N-D)}$ values in Figure 3).

This destabilization in the two-state stacking ⇆ destacking equilibrium (that is the shift toward destacking) is becoming less and less effective because the repulsive anion(G^-)−dipole-($Im^{\delta-}$) interactions are counteracted more and more steadily by the attractive atom−$\pi\sigma$ and anion(G^-)−π/dipole($Py^{\delta+}$) interactions as the RNA chain length increases. This is indeed evidenced by the fact that not only the terminal 1-cytosinyl of p**C**, but also the 9-adeninyl of the immediate neighbor p**A**^{1}p (comparing GpApC with tetramer, pentamer, and hexamer) or p**A**^{2}p (comparing pentamer and hexamer) showed reduced $\Delta\delta_{(N-D)}$ (for δH8A) with increase of the RNA chain length.

Thus, the basis for the observation of the titration curve of the marker protons (H8, H2, and H5/H6) is a pH-dependent response of the relative destacking or the stacking process as a result of competing electrostatic interactions through the ssRNA helix.

It is noteworthy that even in the dimers,[4d] such GpA (**2a**) or ApG (**2b**), the generation of 9-guanylate ion causes a general deshielding [$\Delta\delta_{(N-D)}$] of the H8 proton (and δH2 is non-responding) of the neighboring 9-adeninyl group, which suggests that a destacking due to the Coulombic repulsive anion(G^-)−dipole($Im^{\delta-}$) interaction has taken place in the alkaline pH.

Comparison[19]of oligomerization shift in N and D states of the oligo-RNA with respect to the appropriate monomeric units (**1a**−**g**) shows that as the stacking increases, the anion(G^-)−π/dipole($Im^{\delta-}$) interaction becomes weaker (Tables S1 and S2 in Supporting Information).

Conclusions

(1) The pseudoaromatic nucleobases in the hexameric RNA **8** as well as other oligo-RNAs **4**−**7** constitute an electronically coupled heterocyclic system right across the pH range, 6.7−12.1. The specific generation of a single guanylate ion in the hexameric RNA molecule allowed us to demonstrate that the electrostatic atom−$\pi\sigma$ interaction indeed extends from the first to sixth nucleotide in a single-stranded hexameric RNA in the neutral state. This also shows that the strength of the stabilizing stacking interaction is strongest under the quasi-physiological condition at the neutral state. The transmission of ΔG°_{pKa} from the 5′-guanin-9-yl (or 9-guanylate ion) to the 3′-end nucleobase in the hexameric RNA **8** shows the cross-modulation of the pseudoaromatic character of the nearest neighbors by electrostatic interaction.

(2) The stability of the stacked helical RNA conformation is reduced by the destabilizing anion(G^-)−π/dipole($Im^{\delta-}$) interaction as a result of the generation of the 9-guanylate ion. This destabilizing effect in the deprotonated RNA becomes less pronounced as the RNA chain length increases because of opposing atom−$\pi\sigma$ interaction (major) as well as minor anion-(G^-)−π/dipole($Py^{\delta+}$) interactions. This is quite similar to the polar−π effect found between ions and arene,[7e,f] such as carboxylate−arene interactions[7f] and trimethylammonium ion−arene interactions.[7e] The 9-guanylate ion has a maximal destack-

(18) Leninger, A. L.; Nelson, D. L.; Cox, M. M. *Principles of Biochemistry*, 2nd ed.; Worth Publishers Inc.: New York, 1993.

(19) At the neutral pH, the difference of magnetic shielding ($\Delta\delta_{N(M-O)} > 0$) found in oligomers (*O*) with respect to the monomers (*M*), GpEt (**1a**) and EtpApEt (**1f**) and EtpC (**1g**), results from the cross-modulation of the pseudoaromatic character owing to the offset-stacked coupled aromatic heterocycles within a polyanionic sugar−phosphate backbone. Comparison of $\Delta\delta_{N(M-O)}$ and $\Delta\delta_{D(M-O)}$ as well as of $\Delta\delta_{(N-D)}$ for cytosin-1-yl (p**C**) at the 3′-terminal showed that the stacking propensity of p**C** increases with the chain length (Tables S1 and S2 in the Supporting Information), having maximal upfield shift in the hexameric-RNA at both the neutral as well as in deprotonated states. Similarly, the stacking propensity of the pA^{2}p and pA^{3}p also increases for hexameric-RNA compared to pentameric-RNA (**7** and **8**) as a function of pH, which is consistent with the observed reduction of $\Delta\delta_{(N-D)}$. It is noteworthy that the relative stacking abilities of **2**−**8** are reduced at the deprotonated state compared to that in the neutral state [$\Delta\delta_{N(M-O)} > \Delta\delta_{D(M-O)}$, decrease of $\Delta\Delta\delta_{N-D}{}^{M-O}$ from **2** to **8**, Tables S1 and S2 in the Supporting Information]. It, therefore, shows that the stabilizing offset stacking through electrostatic atom−$\pi\sigma$ and ion−dipole interactions increases most in the hexameric-RNA, which means that the stacking in hexamer opposes the anion(G^-)−π/dipole($Im^{\delta-}$) interaction (causing destacking) more efficiently than in the dimeric-, trimeric-, tetrameric-, or pentameric-RNA.

ing effect up to the third nucleobase along the ssRNA chain, and then the effect diminishes considerably.

(3) The magnitude of the chemical shift change in any of the aromatic protons in either of the two coupled nucleobases differs in a variable manner depending upon the geometry of stacking, electron density around the heteroatom, as well as the sequence context, which is evident from the relative chemical shift changes of the aromatic marker protons as well as from their comparison with the monomeric units. Thus, the physicochemical character (i.e., the cross-modulation of pseudoaromaticity) of an individual nucleobase in an oligonucleotide is determined in a tunable manner, depending upon both the geometry and the strength of the nearest-neighbor interaction.

(4) The pH titration studies with the GpA^{1}pA^{2}pA^{3}pA^{4}pC (**8**) showed that the pK_a of N^1-H of 9-guaninyl from its own δH8G (pK_a 9.76 ± 0.01), δH8A^1 (pK_a 9.65 ± 0.01), and δH2A^1 (pK_a 9.80 ± 0.01) of the p**A**^{1}p moiety, δH8A^2 (pK_a 9.95 ± 0.01) and δH2A^2 (pK_a 10.5 ± 0.07) of the p**A**^{2}p moiety, δH2A^4 (pK_a 9.66 ± 0.01) of p**A**^{4}p moiety, and δH6C (pK_a 10.18 ± 0.03) of the terminal p**C**-3′ moiety. Thus, the pK_a of 5′-**G**p residue from its own δH8G varies only slightly (from 9.76 ± 0.02 to 9.88± 0.01) in the oligo-RNAs **5**−**8**, which should be compared with the pK_a of 9.25 ± 0.01 for GpEt (**1a**), pK_a of 9.17 ± 0.02 for GpA (**2a**), pK_a of 9.56 ± 0.01 for GpC (**3a**), pK_a of 9.45 ± 0.02 for CpG (**3b**), and pK_a of 9.57 ± 0.01 for 5′-EtpG (**3b**). The variation of pK_as for 5′-**G**p residue from *other* aromatic marker protons in the hexamer is, however, more pronounced (from 9.65 ± 0.02 to 10.5 ± 0.12) (Table 1). This variation of pK_as (ΔpK_a ± 0.9) in the hexamer represents a $\Delta\Delta G^\circ_{pKa}$ of ca. 5.1 kJ mol^{-1}, which has been attributed to the variable strength of electrostatic interactions[4d,e] between the electron densities of the involved atoms in the offset stacked nucleobases as well as with that of the phosphates.

(5) The net result of obtaining pK_as of a single ionization point from all marker protons of each nucleotide residue is that it allows us to experimentally examine the microscopic change of the electronic environment around each constituent nucleobase along the RNA chain in a stepwise manner with considerable accuracy without having to make any assumptions. Specific isotope labeling at various sites (i.e., nonuniform labeling) may help in solving the resonance overlapping problems while measuring the pH-dependent chemical shifts of larger biologically active oligo-RNA (depending upon its stability in the pH range to be studied) in understanding the RNA structure−function, in general.

(6) The ΔG°_{pKa} for 9-guaninyl from different marker protons varies (Table 1) from 55.6 ± 0.1 to 56.0 ± 0.1 kJ mol^{-1} for **G**$^-$pApA (**4**),[4e] 56.4 ± 0.1 kJ mol^{-1} for **G**$^-$pApC (**5**),[4e] 55.3 ± 0.1 to 56.2 ± 0.1 kJ mol^{-1} for **G**$^-$pApApC (**6**), 54.7 ± 0.2 to 57.5 ± 0.2 kJ mol^{-1} for **G**$^-$pApApApC (**7**), and 55.1 ± 0.1 to 59.9 ± 0.7 kJ mol^{-1} for **G**$^-$pApApApApC (**8**). These values should be compared with the ΔG°_{pKa} of 52.8 ± 0.1 kJ mol^{-1} for G$^-$pEt (**1**),[4d] 52.4 ± 0.1 kJ mol^{-1} for of G$^-$pA (**2**),[4d] and 53.9 ± 0.1 kJ mol^{-1} for CpG$^-$ (**3b**). The differences in ΔG°_{pKa} measured[14a,b,f−h] from 9-guaninyl in **2**−**8** with respect to the monomeric GpEt (**1a**) or 5′-EtpG (**1e**) (i.e., $\Delta\Delta G^\circ_{pKa}$) is a measure of the relative stability of the 9-guanylate ion in the stacked vs destacked state (Table 1) owing to the variable efficiency of the electrostatic interactions (from −1.1 to 3.6 kJ mol^{-1}). On the other hand, the ΔG°_{pKa} measured for 9-guaninyl from the marker protons show the subsequent electrostatic modulation ($\Delta\Delta G^\circ_{pKa} \approx -0.9$ to 7.1 kJ mol^{-1}), depending upon the sequence context as well as the number of phosphates (chain length) of the oligo-RNA chain. The ΔG°_{pKa} is always larger ($\Delta\Delta G^\circ_{pKa} > 0$) in all residues of oligo-RNA than the monomeric GpEt (**1a**) (Table 1) with the exception of GpA (**2a**)[4d] as well as p**G** of ApG (**2b**) and CpG (**3b**). This means that these additional electrostatic contributions originate from the specific chemical nature of the pseudoaromatic nucleobases of the immediate neighbors due to the change of the local electronic microenvironment, in addition to the charge of the 9-guanylate ion, thereby suggesting, for example, that the pseudoaromatic character of all 9-adeninyl groups in the hexamer is not the same.

Implications

(1) The pH titration study offers an in depth understanding of the nature of the electrostatic mediated self-assembly process by simple intramolecular stacking interactions and the conformational dynamics in the single-stranded RNA, which are normally very difficult to quantitate by state-of-the-art NMR spectroscopy.

(2) The generation of a new anionic[10] or cationic[7a−g] center in the ssRNA destabilizes the stacked state in a distance-dependent manner, which can be thermodynamically described using our pH titration procedure. The fact that the pK_a of 9-guaninyl can be observed from the marker protons of other neighboring residues in the hexamer shows that all residues in the hexamer are stacked (except p**A**^{3}p), although stacking geometry cannot be elucidated, mainly because of inadequate NMR data. Since the p**A**^{3}p residue in the hexamer did not respond to the titration; it shows that it is outside the stacking zone of the neighbors, perhaps bulged out and solvated. Thus, pH titration study with NMR in conjunction with structure elucidation by NMR/ab initio or X-ray and subsequent Poisson−Boltzmann calculation[4j] of the surface potential distribution may allow us to map the electrostatic effect in a ssRNA, in general.[4h] This may help us to understand why the sequence context is so important for biological recognition, interaction, and function of RNA in general.

(3) The sequence-dependent modulation of the pseudoaromatic character of the nucleobases in an oligo-RNA would change the ligand binding properties both by weak interactions (electrostatic, hydrophobic, van der Waals) as well as by hydrogen bonding interactions as found in the aptamers. We, however, envision that the spread of these electrostatic interactions along the RNA chain would depend on whether the neighboring nucleobases are electronically coupled owing to offset stacking or not (ON−OFF switch).

(4) This sequence-stacking based cross-modulation of the pseudoaromatic character to the nearest neighbor at the ground state is likely to be more pronounced in the helical double-stranded RNAs than in the ssRNA because of the restricted flexibility of the former.

Experimental Section

(A) pH-Dependent ^{1}H NMR Measurement. All NMR experiments were performed in Bruker DRX-500 and DRX-600 spectrometers. The NMR samples for compounds **1**−**8** (Figure 1) were prepared in D_2O solution (concentration of 1 mM in order to rule out any chemical shift change owing to self-association) with $\delta_{DSS} = 0.015$ ppm as internal

standard. All pH-dependent NMR measurements have been performed at 298 K. The pH values [with the correction of deuterium effect] correspond to the reading on a pH meter equipped with a calomel microelectrode (in order to measure the pH inside the NMR tube) calibrated with standard buffer solutions (in H_2O) of pH 7 and 10. The pD of the sample has been adjusted by simple addition of microliter volumes of NaOD solutions (0.5, 0.1, and 0.01 M). The assignments for all compounds have been performed on the basis of selective homo- (^{1}H) and heteronuclear (^{31}P) decoupling experiments for **3a** as well as using ^{1}H NOESY, ^{1}H COSY, ^{31}P decoupled ^{1}H COSY, TOCSY, and ^{31}P−^{1}H correlation spectroscopy for **6**−**8** at 298 and 283 K at neutral pH (see Supporting Information). All ^{1}H spectra have been recorded using 128 K data points and 64 scans. All NOESY spectra for **6**−**8** (see the Supporting Information for details) were recorded in a 600 MHz spectrometer with a mixing time (τ_m) of 800 ms. For each FID of NOESY, ^{1}H DQF−COSY, ^{31}P decoupled ^{1}H DQF−COSY, and TOCSY spectra, 64 scans were recorded with a delay of 2s and the data were zero-filled to 4 × 1 K in the t_1 and t_2 directions, then Fourier transformed, phase adjusted, and baseline corrected in both dimensions using polynomial function. The ^{31}P−^{1}H correlation spectroscopy experiment was performed in the absolute magnitude mode using 64 scans with a delay of 2s and then zero-filled to 1 × 1 K data points in the t_1 and t_2 directions, then Fourier transformed, phase adjusted, and baseline corrected in both dimensions using polynomial functions.

(B) pH Titration of Aromatic Protons in 1−8. See refs 4c and 4d for details of the titration profile of GpEt (**1a**), GpA (**2a**), ApG (**2b**), GpA^{1}pA (**4**), and GpApC (**5**). The pH titration studies (pH 6.9−12.1) for isomeric GpC (**3a**) and CpG (**3b**) consist of ∼28 data points (see Figure 2). Similarly, the pH titration studies for GpA^{1}pA^{2}pC (**6**) (pH 7.1−11.8); GpA^{1}pA^{2}pA^{3}pC (**7**) (pH 7.1−11.7), and GpA^{1}pA^{2}pA^{3}pA^{4}pC (**8**) (pH 6.7−12.2) consist of ∼25−33 data points (see Figure 2). The corresponding Hill plots for **3a**, **3b**, and **6**−**8** are given in the Supporting Information (Figure S1 in Supporting Information), and the pK_as shown in Table 1 have been calculated from Hill plot analyses (see section C for details).

(C) pK_a Determination. The pH-dependent [over the range of pH 6.7−12.2, with an interval of pH 0.2−0.3] ^{1}H chemical shift (δ, with error ± 0.001 ppm) for **6**−**8** shows a sigmoidal (having an average of 20 different pH-dependent chemical shifts in each titration profile) behavior [Figure 2]. The pK_a determination is based on the Hill plot analysis[11a,12b,14e] using $pH = \log((1 - \alpha)/\alpha) + pK_a$, where α represents a fraction of the protonated species. The value of α is calculated from the change of chemical shift relative to the deprotonated (D) state at a given pH ($\Delta_D = \delta_D - \delta_{obs}$ for deprotonation, where δ_{obs} is the experimental chemical shift at a particular pH) divided by the total change in chemical shift between neutral (N) and deprotonated (D) state (Δ_T). Thus, the Henderson−Hasselbalch-type equation[11a,14e] can then be written as $pH = \log((\Delta_T - \Delta_D)/\Delta_D) + pK_a$. The p$K_a$ is calculated from the linear regression analysis of the Hill plot [Figure S2 in Supporting Information].

(D) pH-Dependent Sugar Conformation and Gibbs Free Energy [$\Delta G^\circ_{North/South(298K)}$] Calculations. The conformational analyses of the furanose moiety of **1a**, **2a**, **3a**, and **4**−**8** in the N and D states of the two-state 3′-*endo*-2′-*exo* (North-type) ⇆ 2′-*endo*-3′-*exo* (South-type) pseudorotational equilibrium[11] have been performed by using the relation %North-type = $100(7.9 - {}^3J_{1'2'})/6.9$.[11c] Figure 4 shows the bar plot of %North-type pseudorotamer population (error of ±2%) at the N and D states as well as their differences (D − N). The free energies [$\Delta G^\circ_{North/South(298K)}$, in kJ mol^{-1}] have been calculated using Gibb's equation: $\Delta G^\circ_{North/South(298K)} = -RT \ln K$, where $K = (x_{North}/x_{South})$; x_{North} and x_{South} are the mole fraction of North-type and South-type pseudorotamer, respectively. Hence, the negative $\Delta G^\circ_{North/South(298K)}$ implies relatively more North-type conformational population, so more stabilization due to stacking[4d,13b,d] (see Table S3 in Supporting Information for $^3J_{1'2'}$ values).

(E) Calculations of the Dimerization and/or Oligomerization Shift. Dimerization and/or oligomerization shifts[13b] are calculated for the individual nucleotide residues in a dimer (d) and/or oligomer (O) with respect to the monomeric (M) counterparts [$\Delta\delta_{N(M-d)}$ and/or $\Delta\delta_{N(M-O)}$ as well as $\Delta\delta_{D(M-d)}$ and/or $\Delta\delta_{N(M-O)}$, respectively] at the neutral (N) and deprotonated (D) states.[19]

Acknowledgment. Generous financial support from the Swedish Natural Science Research Council (Vetenskapsrådet), the Stiftelsen för Strategisk Forskning, and Philip Morris Inc. is gratefully acknowledged.

Supporting Information Available: Table S1: Dimerization and oligomerization shift estimated from ^{1}H chemical shift at the neutral (N) state at 298 K for aromatic protons of compounds **2a**, **3a**, and **4**−**8** using appropriate monomeric reference compounds (**1a**, **1f**, or **1g**). Table S2: Dimerization and oligomerization shift estimated from ^{1}H chemical shift at the deprotonated (D) state at 298 K for aromatic protons of compounds **2a**, **3a**, and **4**−**8** using appropriate monomeric reference compounds (**1a**, **1f**, or **1g**). Table S3: Endocyclic $^3J_{1'2'}$ values for compounds **1a**, **2a**, **3a**, and **4**−**8** at 500/600 MHz. Figure S1: pH-dependent titration profile of the aromatic protons for compounds **1b**−**e**, **3a**, and **3b** (see Experimental Section for methodology). Figure S2: Hill plot analysis of the pH-dependent chemical shifts of the aromatic protons for compounds **1b**−**e**, **3a**, **3b**, and **6**−**8** giving the pK_a of nucleobase (see Experimental Section for methodology). Figure S3: Panels A, B, and C show stack plots of the pH-dependent ^{1}H NMR chemical shifts of aromatic protons for compounds **6**−**8** [only 10−12 pHs (including two plateaus at two extreme pHs) are shown out of total ∼25−30 pHs, see Experimental Section for details]. Figure S4: Panels A1−5, B1−6, and C1−6 show NMR assignments for compounds **6**−**8**. The 2D NMR spectra for compounds GpA^{1}pA^{2}pC (**6**, panels A1−5) GpA^{1}pA^{2}pA^{3}pC (**7**, panels B1−6), and GpA^{1}pA^{2}pA^{3}pA^{4}pC (**8**, panels C1−6). Panels A1, B1, and C1 are for TOCSY. Panels A2/A3, B2/B3, and C2/C3 are for DQF−COSY. Panels A4, B4/B5, and C4/C5 are for NOESY. Panels A5, B6, and C6 are for ^{31}P−^{1}H correlation spectroscopy. The connectivity and proton assignments are shown in each spectrum. See any current masthead page for ordering information and Web access instructions.

JA034651H